Bayesian design of concrete with amortized Gaussian processes and multi-objective optimization

Olivia P. Pfeiffer[1,‖], Kai Gong[1,‖], Kristen A. Severson[2,3,4], Jie Chen[3,4], Jeremy R. Gregory[5], Soumya Ghosh[3,4] Richard T. Goodwin[6], and Elsa A. Olivetti[1,*]

[1] Department of Materials Science and Engineering, Massachusetts Institute of Technology, Cambridge, MA, USA

[2]Microsoft Research, Cambridge, USA (current)

[3]IBM Research, Cambridge, MA, USA

[4]MIT-IBM Watson AI Lab, Cambridge, MA, USA

[5]MIT Climate and Sustainability Consortium, Massachusetts Institute of Technology, Cambridge, MA, USA

[6] IBM T.J. Watson Research Center, Yorktown, NY, USA

[‖]These authors contributed equally to this work.

[*]Corresponding author: elsao@mit.edu

Abstract

Here, we present a computational framework, combining machine learning models with inverse optimization, which can accelerate and optimize concrete mix design with respect to climate impact and/or cost. Our approach leverages a novel amortized Gaussian process (GP) model trained on a large industry dataset to predict concrete strength based on mix proportions. The resulting GP model has an R^2 value, RMSE, and MAPE of ∼0.88, ∼909 psi (6.3 MPa), and ∼10.8%, respectively. We integrated the GP model with an inverse optimization scheme to predict optimal mix designs that minimize cost and/or climate impact. The results show that this integrated framework can generate reasonable concrete mixes that offer up to ∼30% and ∼60% reduction in cost and climate impact, respectively, compared with industry mixes with similar 28-day strength. This study highlights the potential environmental and economic benefits of data-driven approaches to design and optimize concrete mixes.

Keywords: Concrete mix design, Industrial data set, Machine learning,

Gaussian process, Multi-objective optimization

1. Introduction

Concrete is the most widely used building material in the world, with a global annual production of approximately 30 billion metric tons [1]. Although concrete has a lower carbon and energy footprint than almost all construction materials on a unit mass basis [2, 3], the sheer scale of concrete production and usage brings along huge environmental burdens. It has been estimated that cement and concrete production is responsible for ∼8% of global CO_2 emissions [4, 1], rendering it an important consideration for the global decarbonization effort.

To date, numerous research efforts have been dedicated to lowering the CO_2 emissions of cement and concrete production. According to the International Energy Agency, one of the most promising mitigation strategies is to partially replace ordinary Portland cement (OPC) with supplementary cementitious materials (SCMs) with significantly lower carbon footprints [5], e.g., fly ash (FA) from coal-fired power plants, blast-furnace slag (BFS) from steel production, and silica fume (SF) from silicon and ferrosilicon alloy production. These three SCMs have already been widely adopted by the concrete industry, as shown by the published industry concrete data in the literature [6, 7, 8] as well as those presented here. In addition to lowering CO_2 emissions and cost, the inclusion of SCMs in concrete can also increase the long-term strength of concrete, improve durability, and mitigate permeability, among many other effects [9, 10].

The use of SCMs, together with many organic and inorganic admixtures often incorporated to tailor concrete properties, render modern concrete a highly complex materials system. This complexity has led to industrial concrete mixture design based mostly on prescriptive and trial-and-error approaches [11], which are labor-intensive, time-consuming, and costly, yet result in sub-optimal designs. Given that the existing high-quality BFSs and FAs are already highly utilized in concrete production and that researchers are actively exploring a vast number of additional SCM sources [9, 10] and other concrete additives (e.g., fillers and fibers), modern concrete materials are likely to be increasingly more complex in the future. This expected increase in complexity, together with the increasing need to lower concrete emissions, call for new design strategies that will enable rapid optimal mixture designs (e.g., achieving lower environmental impacts and cost while still meeting structural performance requirements) for any given applications. For this purpose, data-driven machine learning (ML) methods offer potential due

to their ability to capture complex interactions among input features (e.g., individual concrete constituents) along with their correlations with target output (e.g., concrete properties).

An increasing number of studies have explored ML as a means to predict concrete properties (including mechanical strength) as a function of their mix proportions, as reviewed recently by Ben Chaabene et al. [12], Nunez et al. [13], and Li et al. [14]. As seen in these reviews, most existing ML studies on concrete strength prediction are based on small lab datasets (typically less than ∼300 observations), with only a handful of them having a size greater than 1,000 observations [12, 13, 14]. The highest use larger data set (∼1,030 observations) was compiled by Yeh over two decades ago [15] based on seventeen early experimental studies, which contains concrete compressive strength at different ages along with the quantities of cement, BFS, FA, water, superplasticizer, and fine and coarse aggregate.

Although these studies based on small lab datasets are highly valuable, larger datasets are often needed to develop more robust and reliable ML models. For applications to real-world industry concrete mixes, ML models developed based on large industry datasets are needed, which are inherently more complex and have higher uncertainties than data collected under controlled lab conditions. However, to this date, few ML studies on concrete have explored large industrial datasets. Exceptions [6, 7, 8] include a recent study by Young et al. [6], which presented several ML models to predict concrete compressive strength using an industrial dataset (roughly 10,000 observations collected at job sites) consisting of eight input features (specifically, water/cement ratio, FA, coarse aggregate, fine aggregate, air-entraining admixture, water-reducing admixture, air content and cement). They found that the overall model performance was noticeably poorer on the industrial data set (R^2 values of ∼0.6) than on the Yeh data set, where R^2 values above ∼0.80 (and ∼0.90) are reported in their study [6] (and many previous studies [16, 17, 18, 19, 20]). The lower model performance for industry data (compared with the lab data) was also observed by Rousseau et al. [7]. This discrepancy in performance between industry- and lab-based data sets has been attributed to the higher level of noise in the industrial dataset from higher uncertainty or uncontrolled/unreported process variables during the process of proportioning, mixing, casting, and testing [6]. Young et al. [6] suggested that future work should aim to expand the size of the data and incorporate a wider set of input variables for improved results when using industrial data.

In light of this need, here we present a large industrial concrete dataset collected by a concrete producer at various job sites across the United States in 2017-2020, containing 9,296 concrete mixes with 38,332 compressive strength measurements. Using this dataset, we built a novel amortized Gaussian process (GP) model with embedded domain knowledge (based on our early work [21]) to predict concrete strength and strength trajectories (i.e., output target) as a function of water/cementitious (w/cm) ratio and 12 constituent quantities (i.e., input features). We chose the GP model (as opposed to the more commonly used random forest (RF) and neural network (NN) models) because the problem of predicting concrete strength (which evolves as a function of time) is well-suited to time-series analysis methods such as the GP model.

We integrated this strength model (i.e., amortized GP) into an optimization framework with nonlinear constraints, where the mix design is optimized on two criteria (i.e., climate impact and cost) for specified 28-day target strengths. The minimization of both cost and climate impact is different from most existing optimization studies presented in the concrete literature [6, 22, 23, 24, 25, 26, 27, 28, 29, 30], which minimize either cost or climate impact (sometimes in combination with performance objectives (e.g., maximize strength [28, 30, 31])). For example, Young et al. [6] presented an optimization procedure based on a NN model to minimize mixture cost subject to both target strength constraints and target embodied carbon impact. Several exceptions [32, 33] have simultaneously minimized cost and climate impact using metaheuristic algorithms; however, they are based on smaller and simpler lab datasets (30-344 measurements).

We use the amortized GP model to predict the strength trajectories of the identified optimal mixes to check the development of early-age strength. We have also explored the impact of several scenarios (i.e., increasing unit prices for two widely adopted SCMs (BFS and FA)) on the optimization outcome. We demonstrate the potential of incorporating prediction uncertainty from the GP model into the inverse optimization framework. This study highlights the applicability of data-driven approaches in optimizing real-world concrete mixes, revealing the potential for both cost and climate impact reductions. The inclusion of cost in the optimization framework could be an important driver for the concrete industry to adopt unconventional yet more sustainable mix designs.

2. Industrial Concrete Dataset

The concrete dataset used in this study was provided by an industrial concrete producer, and contains data collected for different projects over a period of ∼3.5 years (2017-2020) across the United States. We aimed to perform minimal pre-processing in the dataset. The raw dataset has mixture quantities for over 40 constituents, including two types of Portland cement (ASTM Type II and Type I/II cements), nine FAs (density of 2.52-2.8 g/cm^3), five BFSs (density of 2.85-2.95 g/cm^3), and coarse aggregates of different size (e.g., 1 1/2, 3/4, 1/2 and 3/8 inches), type (limestone and trap rock) and origin. This diversity of materials used highlights the complexity of industrial concrete datasets as compared to the lab-based concrete datasets used in most existing ML studies (as summarized recently by Ben Chaabene et al. [12] and Li et al. [14]). These constituent sub-categories (over 40 in total) are collapsed into 12 main categories which trade off between data availability for each constituent type (e.g., about 30% of the data contain one type of FA while several other FAs were used only in less than 1% of the data, plus no chemistry and mineralogy information is available for OPCs, BFSs and FAs) and a loss of descriptive information. The resulting 12 major constituent categories are coarse aggregate, fine aggregate, water, cement, FA, BFS, SF, and high-range water-reducing (HRWR), water-reducing, accelerating, air-entraining, and other (e.g., viscosity modifying) admixtures. Obvious outliers, likely data-entry errors, were removed. For example, some 28-day strength data are significantly lower (some up to 10 times lower) than the corresponding 28-day design strength, possibly due to recording or experimental errors; these instances are manually identified and removed.

The final dataset consists of 9,296 concrete mixes, each with a varying number of compressive strength measurements at different ages (range 1–26, average 4.1 measurements per mix), for a total of 38,332 measurements, yielding one of the largest concrete mixture and strength dataset studied. The other two reported large industrial concrete strength data sets are from Zhang et al. [8] (12,107 strength measurements on 25 concrete mixes) and Young et al. [6] (9,994 strength measurements). For the purposes of modeling, each mixture is represented by a 13-dimensional vector: the water-to-cementitious material (w/cm; cementitious material = cement + SCMs) ratio and the quantities of the 12 major constituent categories in units of mass per cubic yard (CY) of concrete (1 CY = 0.76 m^3). Table 1 summarizes the statistics of the final dataset, and Fig. 1 displays the 28-day

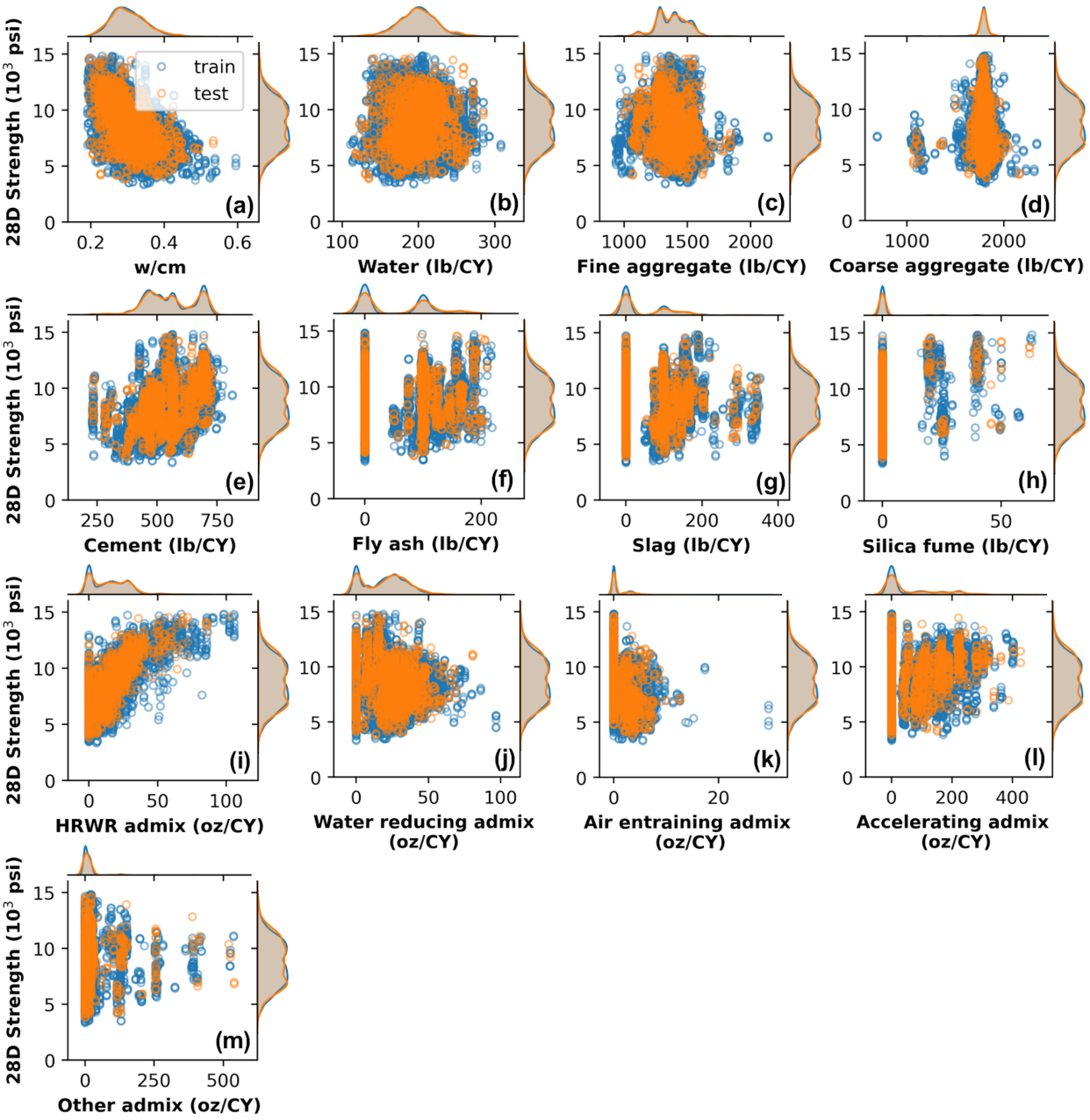

Figure 1: Visualization of 28-day compressive strength (in psi) as a function of each of the 13 variables in the 80% training (blue) and 20% testing (orange) sets: (a) w/cm ratio, and quantity of (b) total water, (c) total fine aggregate, (d) total coarse aggregate, (e) total cement, (f) total fly ash (FA), (g) total blast furnace slag (BFS), (h) total silica fume (SF), (i) total high-range water-reducing (HRWR) admixture, (j) total water-reducing admixture, (k) total air entraining admixture, (l) total accelerating admixture, and (m) total other admixtures (e.g., viscosity modifying admixtures). The histogram distributions of strength and each variable in both the training and testing sets are also given. The constituent quantities are given in either pound per cubic yard (lb/CY = $\sim$0.59 kg/m^3) or ounce per cubic yard (oz/CY = $\sim$0.037 kg/m^3) of concrete, while strength is given in pound-force per square inch (psi = $\sim$0.0069 MPa).

compressive strength (i.e., target) as a function of each of the 13 variables (i.e., input features), which clearly shows that there is significant variation in the constituent quantities in the dataset. For example, the w/cm ratio ranges from ∼0.2 to ∼0.6, while the 28-day concrete strength varies between ∼3,000 and ∼15,000 psi (∼23 and ∼102 MPa). This large variability of our industry dataset is further illustrated by the principle component analysis in Fig. S1 of Appendix, where the industry data is clearly seen to occupy a wider design space (higher variations among designs of different mixes) than the Yeh dataset [15].

Furthermore, Fig. 1 show that the 28-day strength is generally inversely correlated with w/cm ratio (Fig. 1(a)) and positively correlated with the total HRWR admixture (Fig. 1(i)). The inverse correlation between strength and w/cm ratio is consistent with domain knowledge and the published industry data [6, 34, 35]. However, the positive correlation in Fig. 1(i) was not observed by Young et al. [6] due to the lack of HRWR admixture in their industry dataset. This positive correlation can be attributed to the fact that high-strength concrete mix design often requires the use of HRWR admixture to maintain workability for low w/cm concrete (see the overall inverse correlation between the quantity of HRWR admixture and w/cm ratio in Fig. S2 of Appendix for our dataset). The correlations of other variables with 28-day strength are less obvious, even for SF (Fig. 1(f)) and air-entraining admixture (Fig. 1(k)), which are known to increase [36] and decrease [37] concrete strength, respectively. Furthermore, there are significant variations in concrete strength at the same level of w/cm (Fig. 1(a)) or HRWR admixture (Fig. 1(i)), which suggests that other variables also influence the 28-day strength. These observations are consistent with the industry data presented in ref. [6], further highlighting the complexity (and non-linearity) of industry data.

We use 80% of the data for training the model and the remaining 20% for testing the model (obtained via a random training-testing split). To avoid leakage between the training and testing sets, we have partitioned the data based on mixture ID, such that a given concrete mixture with multiple strength observations (including measurements at different ages and repeated measurements at the same age) appears only in the training or testing set (or vice versa), but not both. As shown in Fig. 1, the distributions of each feature in both the training and testing sets are similar, suggesting that both sets are representative of the overall data set. All values have been z-scored prior to model training by subtracting the mean and dividing by the standard

Table 1: Summary statistics of the processed industrial data set (based on 1 cubic yard ($\sim$ 0.76 m^3) of concrete), including the 12 major constituent categories and some selected attributes. lb = pound; oz = ounce; psi = pound force per square inch. 1 lb = $\sim$ 0.45 kg; 1 oz = $\sim$ 0.028 kg; 1000 psi = $\sim$ 6.9 MPa.

	Mean	**St. dev**	**Min**	**25%**	**50%**	**75%**	**Max**
Coarse aggregate (lb)	1779.3	97.4	690.4	1767.3	1790.0	1810.0	2336.8
Fine aggregate (lb)	1376.2	127.4	847.1	1285.5	1382.0	1468.9	2136.5
Cement (lb)	554.4	105.4	228.9	468.9	553.3	664.0	850.0
Water (lb)	199.0	24.6	107.6	183.5	199.5	214.7	307.9
Slag (lb)	54.4	71.4	0.0	0.0	0.0	101.1	351.7
Silica fume (lb)	1.5	7.0	0.0	0.0	0.0	0.0	62.9
Fly ash (lb)	55.7	60.0	0.0	0.0	0.0	100.6	253.4
HRWR adm. (oz)	15.8	14.9	0.0	0.0	14.9	26.9	105.6
Water red. adm. (oz)	20.1	15.3	0.0	5.9	20.9	30.7	96.5
Accelerating adm. (oz)	63.1	89.9	0.0	0.0	0.0	116.0	426.7
Air-entraining adm. (oz)	1.1	1.8	0.0	0.0	0.0	2.1	29.6
Other adm (oz)	16.4	43.1	0.0	0.0	0.0	16.0	768.0
w/cm	0.30	0.05	0.19	0.27	0.30	0.33	0.60
28-day strength (psi)	8686	2042	3340	7080	8650	10270	14830
FA ratio	0.08	0.09	0.00	0.00	0.00	0.15	0.40
SL ratio	0.09	0.11	0.00	0.00	0.00	0.17	0.60
SF ratio	0.00	0.01	0.00	0.00	0.00	0.00	0.08
SCM ratio	0.17	0.09	0.00	0.13	0.16	0.21	0.60
Agg ratio	0.73	0.03	0.62	0.71	0.73	0.75	0.79
AEA/100*cement	0.21	0.35	0.00	0.00	0.00	0.43	5.69

deviation.

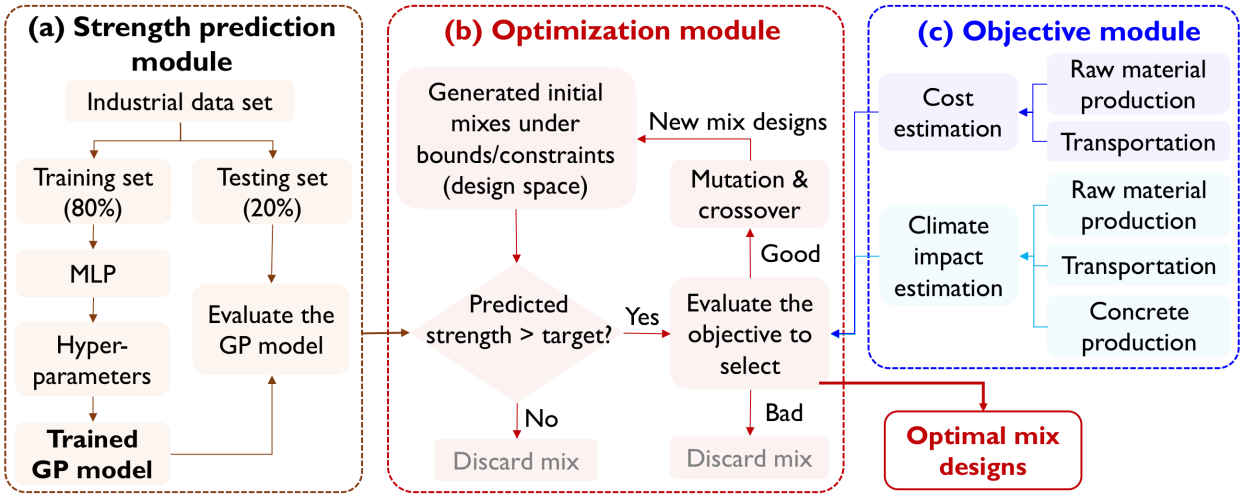

Figure 2: Schematic overview of the proposed computational frameworks consisting of three modules: (a) a strength prediction module (see Section 3.1), (b) an optimization module (see Section 3.3) and (c) an objective estimation module (see Section 3.2).

3. Computational Methods

Fig. 2 presents a schematic overview of the computational framework used to generate optimal concrete mix designs. It consists of three modules: (a) a strength prediction module based on a GP model which enables concrete strength prediction as a function of the mix proportions and time, (b) an optimization module that generates and searches for optimal mix designs, and (c) an objective module that calculates the cost and climate impact of any given mix design. In the following sections we describe each of the modules.

3.1. Gaussian process regression model for prediction of strength trajectories

To ensure specified compressive strength requirements are met, we developed a model which can make strength predictions given the mix design and time. We select Gaussian processes (GPs) for three reasons. First, GPs are well-suited for time series predictions [38], particularly in cases of irregular sampling, as is true for our industrial concrete dataset. Irregular sampling refers to a lack of consistency in time points, e.g. one mix may be measured at 3 and 28 days while another is measured at 7 and 14 days. GPs are also able to incorporate domain knowledge into the time series model as a prior.

Second, compared with other ML models, such as support vector regression and RF, GPs return not only mean predictions but also variance as an uncertainty measure, producing more informative estimates of the compressive strength. Such information can be useful for more robust optimization results. Third, GP models update their forecast based on additional observations, which can possibly accelerate mix development. These advantages are further described below.

A GP provides flexibility in modeling because it is a distribution over functions. Formally, a GP is a stochastic process such that any finite collection of random variables indexed by time t is jointly Gaussian. Characterizing a GP requires specifying a mean function $m(t)$ and a covariance function $k(t, t')$. We can then write the Gaussian process as

$$f(t) \sim \mathcal{GP}(m(t), k(t, t')). \tag{1}$$

We model the compressive strength y as a random function, perturbed by independent noise ϵ:

$$y = f(t) + \epsilon(t), \tag{2}$$

where

$$\epsilon(t) \sim \mathcal{N}(0, \sigma_t^2). \tag{3}$$

When a set of observations, $\mathcal{D} = \{(t_m, y_m)\}_{m=1}^{M}$, is available, conditioned on such a dataset, the posterior distribution over functions is yet another Gaussian process. Moreover, by marginalizing over the posterior Gaussian process, the predicted targets adopt a posterior predictive distribution that is also Gaussian:

$$\mathbf{y}_*|\mathcal{D} \sim \mathcal{N}(\overline{\mathbf{y}}_*, \overline{\mathbf{V}}_{**}), \tag{4}$$

where

$$\overline{\mathbf{y}}_* = \mathbf{m}_* + \mathbf{K}_*(\mathbf{K} + \sigma^2\mathbf{I})^{-1}(\mathbf{m} - \mathbf{m}_*), \tag{5}$$

$$\overline{\mathbf{V}}_{**} = \mathbf{K}_{**} - \mathbf{K}_*(\mathbf{K} + \sigma^2\mathbf{I})^{-1}\mathbf{K}_*^T. \tag{6}$$

Here, $\mathbf{m} = [y]$ and $\mathbf{K} = [k(t, t')]$ for all t, t' and y in the observation set; while $\mathbf{m}_* = [m(t_*)]$, $\mathbf{K}_{**} = [k(t_*, t'_*)]$, and $\mathbf{K}_* = [k(t_*, t')]$ for all t_* and t'_* in the prediction set.

In our application, we model each mix using a Gaussian process and select the mean and covariance functions based on domain knowledge. The mean function (see Eq. 7) is chosen to be a log-linear function based on the typical

shape of the trajectory of compressive strength as a function of time. The covariance function (see Eq. 8) is chosen to be the squared exponential, a typical choice for a smooth GP.

$$m(t;\boldsymbol{\theta}) = \theta_1 \log t + \theta_2, \tag{7}$$

$$k(t,t';\boldsymbol{\theta}) = \theta_3 \exp\left(-\frac{(t-t')^2}{2(\theta_4)^2}\right), \tag{8}$$

where $\boldsymbol{\theta} = [\theta_1, \ldots, \theta_4]$ denotes the vector of hyperparameters.

To apply the model, the hyperparameters $\boldsymbol{\theta}$ need to be estimated. We expect the hyperparameters to differ depending on the formulation constituents, $\mathbf{z} \in \mathbb{R}^d$. A standard approach to performing this estimation is to find the values of $\boldsymbol{\theta}$ which optimize the marginal likelihood of observing the data under a particular choice of $\mathbf{z}$. However, as our aim is to propose, probably novel, formulations, there may be little to no data to perform this optimization. Instead, as in [21], we use *amortization*, a concept in the machine learning literature referring to a parameterization of the quantity to be estimated, so that the repeated estimation of the quantity under different scenarios is replaced by a one-time estimation of the parameters of a function which predicts that quantity. To this end, we let the hyperparameters $\boldsymbol{\theta}$ be parameterized by using a multi-layer perceptron (MLP) of the concrete formulation $\mathbf{z}$:

$$\boldsymbol{\theta} = \mathrm{MLP}_{\boldsymbol{\phi}}(\mathbf{z}), \tag{9}$$

where the MLP contains parameters $\boldsymbol{\phi}$. We choose the architecture of the MLP to further encode our domain knowledge by constraining θ_1 to be positive.

Given a collection of formulations and associated strength measurements, $\{\mathbf{z}_i, \mathbf{y}_i, \mathbf{t}_i\}_{i=1}^N$, where $\mathbf{y}_i = [y_{i1}, \ldots, y_{iM_i}]^T$ are the observed strengths at times $\mathbf{t}_i = [t_{i1}, \ldots, t_{iM_i}]^T$, we estimate $\boldsymbol{\phi}$ through maximizing the log-marginal likelihood,

$$\mathcal{L}(\boldsymbol{\phi}) = \sum_{i=1}^{N} \log p(\mathbf{y}_i \mid \mathbf{t}_i, \mathbf{z}_i; \sigma^2, \boldsymbol{\phi}), \tag{10}$$

where the Gaussian probability density p is specified by the mean function $m(t;\boldsymbol{\theta})$ and the covariance function $k(t,t';\boldsymbol{\theta})$, which in turn depend on the formulation $\mathbf{z}$. It is possible to jointly learn ϕ with the noise parameter σ in Eq. 3, however in practice we perform a separate estimation of σ leveraging repeated measurements from the same mix and time point in the industrial dataset.

3.2. Objective estimation

3.2.1. Climate impact of concrete mix design

We estimate the climate impact of a given concrete mixture ($f_g(\mathbf{z}_i)$) on a cradle-to-gate basis using Eq. 11:

$$f_g(\mathbf{z}_i) = \mathbf{g}_m^\intercal \mathbf{z}_i + \mathbf{g}_t^\intercal \mathbf{z}_i + g_p \tag{11}$$

where $\mathbf{g}_m, \mathbf{g}_t$, and g_p denote the GHG emissions associated with raw materials production, transportation, and concrete production, respectively and $\mathbf{z}_i$ is a vector containing constituent quantities for a given concrete mix i .

We use two data sources for the climate impact analysis: the ecoinvent inventory database for raw materials [39] and the life cycle assessment (LCA) report commissioned by the National Ready Mixed Concrete Association (NRMCA) [40] for raw material production and transportation. Environmental product declarations for chemical admixtures provide materials climate impacts estimates [41, 42, 43]. Table 2 shows the climate impact factors associated with the raw material production ($\mathbf{g}_{m,j}$) and transportation ($\mathbf{g}_{t,j}$) of each constituent j in a mixture i (denoted $z_{i,j}$). These factors are measured in CO_2 equivalents (CO_2-eq) per unit mass of constituent, where the global warming potential (GWP) index is used in order to express the total warming effect of all GHGs in terms of CO_2. For example, 1 kg of methane has about 30 times the warming potential of 1 kg of CO_2 over a fixed time period (e.g., 100 years), thus the GWP of methane is about 30. The climate impact associated with the production of 1 CY (~ 0.76 m^3) of concrete (i.e., the g_p in Eq. 11) is calculated as 5.79 kg CO_2-eq using national average statistics and is assumed to be the same for all concrete mixes in the study. The final total climate impact (as given by Eq. 11) is reported in unit of kg CO_2-eq/CY of concrete.

3.2.2. Cost of concrete mix design

We estimate the cost of a concrete mixture per CY (~ 0.76 m^3), $f_c(\mathbf{z}_i)$, using Eq. 12, where the unit costs for raw material production, $\mathbf{c}_m$, and transportation, $\mathbf{c}_t$, are given in Table 3 for each constituent $z_{i,j}$.

$$f_c(\mathbf{z}_i) = \mathbf{c}_m^\intercal \mathbf{z}_i + \mathbf{c}_t^\intercal \mathbf{z}_i \tag{12}$$

The unit price for the constituents (as given in Table 3) are estimated considering several literature studies [6, 48] and the fact that the cost of BFS

Table 2: Summary of the climate impact factors associated with raw materials production ($g_{m,j}$, Eq. 11) and transportation ($g_{t,j}$, Eq. 11) of each constituent j on a mass basis, which are obtained from refs. as indicated in the brackets. The climate impact associated with the production of 1 CY ($\sim$ 0.76 m^3) of concrete (i.e., the g_p term in Eq. 11) is estimated as 5.79 kg CO_2-eq.

j	**Mixture constituent**	**Raw materials production ($g_{m,j}$)**	**Transportation ($g_{t,j}$)**
	Non-admixtures	kg CO_2-eq/kg	kg CO_2-eq/kg
1	Coarse aggregate	0.00503 [39]	0.00728 [40]
2	Fine aggregate	0.00503 [39]	0.00721 [40]
3	Water	0.00212 [39]	0
4	Cement	1.043 [44]	0.02932 [40]
5	Fly Ash (FA)	0.00397 [45]	0.01887 [40]
6	Slag (BFS)	0.14705 [46]	0.01942 [40]
7	Silica fume (SF)	0.00397 [47]	0.01887[!]
	Admixtures	kg CO_2-eq/kg	kg CO_2-eq/kg
8	HRWR	1.884 [43]	0
9	Water reducing	1.884 [43]	0
10	Accelerating	1.3404 [41]	0
11	Air-entraining	0.52805 [42]	0
12	Other	1.884 [*]	0

Note: [!]assumed to be the same as those of FA.
[*]assumed to be the same as the transportation cost of HRWR and Water reducing admixtures.

Table 3: Summary of cost factors used in this study for raw materials production ($c_{m,j}$, Eq. 12) and transportation ($c_{t,j}$, Eq. 12) of each constituent j on a mass basis.

j	**Mixture constituent**	**Raw materials production ($c_{m,j}$)**	**Transportation ($c_{t,j}$)**
	Non-admixtures	\$/kg	\$/kg
1	Coarse aggregate	0.00992	0.005265
2	Fine aggregate	0.00595	0.005075
3	Water	0	0
4	Cement	0.11	0.02729
5	Fly Ash (FA)	0.055	0.01318
6	Slag (BFS)	0.11	0.02402
7	Silica Fume (SF)	0.397	0
	Admixtures	\$/kg	\$/kg
8	HRWR	2.928	0
9	Water reducing	2.928	0
10	Accelerating	2.928	0
11	Air-entraining	2.928	0
12	Other	2.928	0

powder is comparable to OPC. Transportation cost estimates use national average transport distances and quantities reported in [40], and assume costs per ton-mile for truck, rail, ocean, and barge to be \$0.15, \$0.05, \$0.04,and \$0.03, respectively. The cost of water is assumed to be zero, as is often done, e.g. [6], given that its cost is significantly lower than other constituents. The transportation costs for the admixtures and SF are also assumed to be zero, given that they are relatively small compared with the corresponding raw material cost (i.e., if we assume a unit transportation cost of \$0.022/kg for constituents 7-12 in Table 3, this transportation cost is only ∼1-6% of its corresponding material cost, compared with ∼20-85% for constituents 1-6 (excluding water)).

We note that the cost and climate impact factors for individual constituents in Tables 2 and 3 may evolve with time, source and region. Hence, it is important to consider how the optimal mix design may change as SCMs (e.g., FA and BFS) become more expensive, for example, as coal-fired power plants are retired and FA becomes more scarce. Thus, we have studied three cost scenarios in addition to the baseline, as shown in Fig. 3, where we in-

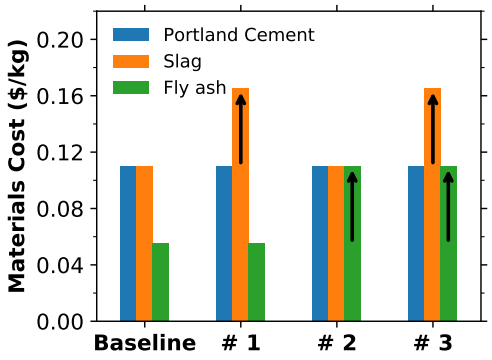

Figure 3: Three studied scenarios with increasing unit prices of slag (Scenario 1), fly ash (Scenario 2), and both slag and fly ash (Scenario 3) from the baseline level.

crease the unit price of BFS (Scenario 1), or FA (Scenario 2), or both BFS and FA (Scenario 3) by \$0.055/kg from the corresponding baseline price.

3.3. Optimization of concrete mix design

3.3.1. Bounds and constraints

In order to improve numerical stability and ensure that the predicted optimal concrete mixtures are feasible, we have imposed some bounds and constraints in the optimization framework, similar to previous concrete optimization studies [6, 32, 49, 28].

Bounds. Both upper and lower bounds are specified for each constituent quantity, along with constituent ratios where appropriate, which are summarized in Tables 4 and 5, respectively. The ratio bounds (e.g., BFS, FA, SF, and SCM ratios and w/cm) are roughly selected based on the ranges of the ratios reported in the original industrial data set (see Table 1). The use of these bounds not only reduces the design feature space to be explored during the optimization (hence lowers the computational cost) but also ensures the feasibility of the predicted individual constituent quantity (i.e., avoiding non-physically high or low values by exploring a design feature space comparable to that of the original industrial data set).

Strength constraint. Using the GP model described in Section 3.1, we obtain the predictions of strength for a given mix design $\mathbf{z}_i$ and age t as expressed using Eqs. 13-14. Note that Eq. 14 is the prior mean function of the GP

Table 4: Densities and lower and upper bounds for each constituent. The density values for the coarse and fine aggregates and each type of SCM are taken as the average of the prevalent sources in the database. The density values of the admixtures are not available in the database, and we used the average values of the available Sika products (https://usa.sika.com/en/construction-products/concrete/concrete-admixtures) for each type of admixture.

j	**Mixture constituent**	**Density** (ρ_j)	**Lower Bound** (LB_j)	**Upper Bound** (UB_j)
	Non-admixtures	g/cm^3	kg (lb)	kg (lb)
1	Coarse aggregate	2.71	415 (700)	2373 (4000)
2	Fine aggregate	2.63	415 (700)	2373 (4000)
3	Water	1.00	18 (30)	593 (1000)
4	Cement	3.15	59 (100)	1780 (3000)
5	Fly Ash (FA)	2.60	0	297 (500)
6	Slag (BFS)	2.92	0	297 (500)
7	Silica Fume (SF)	2.20	0	59 (100)
	Admixtures	g/cm^3	kg	kg (oz)
8	HRWR	1.08	0	7 (200)
9	Water-reducing	1.14	0	7 (200)
10	Accelerating	1.34	0	22 (600)
11	Air-entraining	1.01	0	4 (100)
12	Other	1.10	0	37 (1000)

model (Eq. 7) leveraging the trained MLP (Eq. 9). The constraint as written in Eq. 15 can be interpreted as the following: the mean predicted strength of mixture $\mathbf{z}_i$ at time t (i.e., $f_s(\mathbf{z}_i, t)$) should meet or exceed a minimum specified target strength, s_{min}. In this work, we have considered 6-10 target 28-day strengths (ranging from 4,000 to 13,000 psi (27.6-89.7 MPa) at an increment of 1,000 psi (6.9 MPa)), given the importance of 28-day strength to concrete design and its prevalence in concrete literature. Nevertheless, it is worthwhile for future investigations to explore multiple constraints of strength over time.

$$\boldsymbol{\theta}_i = \text{MLP}(\mathbf{z}_i) \tag{13}$$

$$f_s(\mathbf{z}_i, t) = \theta_{i,1} \log t + \theta_{i,2} \tag{14}$$

$$f_s(\mathbf{z}_i, t) \geq s_{min} \tag{15}$$

We also consider an alternative specification of the strength constraint. As the GP can also predict uncertainty, we frame the constraint as requiring that the predicted strength exceeds the target strength with a specified probability p_c.

$$\boldsymbol{\theta}_i = \text{MLP}(\mathbf{z}_i) \tag{16}$$

$$p(y_i|t, \boldsymbol{\theta}_i, \sigma_t, \phi) \sim \mathcal{N}(m(t; \boldsymbol{\theta}_i), k(t, t'; \boldsymbol{\theta}_i) + \sigma_t) \tag{17}$$

$$p(y_i \geq s_{min}|t, \boldsymbol{\theta}_i, \sigma_t, \phi) \geq p_c \tag{18}$$

where y_i is the predicted strength at 28-day for a given concrete mix (i.e., $f_s(\mathbf{z}_i, 28)$). For additional details, please refer to the appendix.

Volume Constraint. Since all the constituent quantities in the original dataset are given based on one CY (~ 0.76 m^3) of concrete, the volume of the predicted concrete mix design should be approximately one CY. Based on density of individual constituent ρ_j (as given in Table 4) and Eq. 19 (volume based on materials), we have estimated the volume of all concrete mixes in original data set (V_m), which is shown in Fig. 4. We note that the density value of each constituent is taken as the average of the prevalent sources in the database. For example, the coarse aggregate in the database is predominantly ($> 99\%$) limestone aggregate, with density values ranging from 2.65 to 2.71 g/cm^3. The prevalent coarse aggregate used is 3/4 inch ($\sim$1.9 cm) limestone with an average density of 2.71 g/cm^3, which is adopted in Table

4 to represent coarse aggregate density. This simplification (or estimation of density) will induce some uncertainty in the subsequent volume calculation.

In Fig. 4, we observe a peak at ∼0.97 CY with small deviation (mostly smaller than ∼2%) for concrete without air-entraining admixture (AEA), suggesting that these concrete also has a small amount entrained air (about 3%) which is reasonable [50]. The small deviation around the peak is likely caused by the density uncertainty of individual constituents, as mentioned above (e.g., different sources of coarse aggregate have slightly different density values), and the amount of entrained air. For concrete with AEA, the estimated volume peaked at ∼0.93 CY, which suggests the presence of ∼7% entrained air. Furthermore, we observe that the most typical dosage of AEA (oz) per 100 lb of cement (1 lb = 16 oz) in the air-entrained concrete is 0.39 (see Fig. S3 of Appendix). Therefore, we formulate the volume constraint according to Eq. 20, where we assume 7% entrained air when $z_{11}/(z_4/100) \geq 0.39$ while 3% entrained air when $z_{11}/(z_4/100) < 0.39$. For the final volume, we formulate an inequality in the optimization as shown in Eq. 21, which is more attainable, as it can be thought of as a relaxed version of an equality constraint. Furthermore, we have considered an additional scenario when no constraints have been imposed on the AEA (i.e., $V_{final} = V_m + 3\%$). This treatment generates concrete mix designs without AEA, similar to the approach adopted in ref. [6].

Finally, similar to ref. [6], we have also imposed an aggregate volume ratio constraint as given by Eqs. 22 and 23, which is within the range of values adopted in our industrial data (see Table 1). Considering the significantly lower cost and climate impact factors associated with aggregates, the introduction of the aggregate volume ratio constraint of 0.65-0.75 prevents the generation of mixes with an excessive amount of aggregates, which is known to cause workability issue [51].

$$V_m = \frac{z_1}{\rho_1} + \frac{z_2}{\rho_2} + \frac{z_3}{\rho_3} + \frac{z_4}{\rho_4} + \frac{z_5}{\rho_5} + \frac{z_6}{\rho_6} + \frac{z_7}{\rho_7} + \frac{z_8}{\rho_8} + \frac{z_9}{\rho_9} + \frac{z_{10}}{\rho_{10}} + \frac{z_{11}}{\rho_{11}} + \frac{z_{12}}{\rho_{12}} \tag{19}$$

$$V_{final} = \begin{cases} V_m + 0.07, & \text{if } \frac{z_{11}}{z_4/100} \geq 0.39 \\ V_m + 0.03, & \text{otherwise} \end{cases} \tag{20}$$

$$0.99 \leq V_{final} \leq 1.01 \tag{21}$$

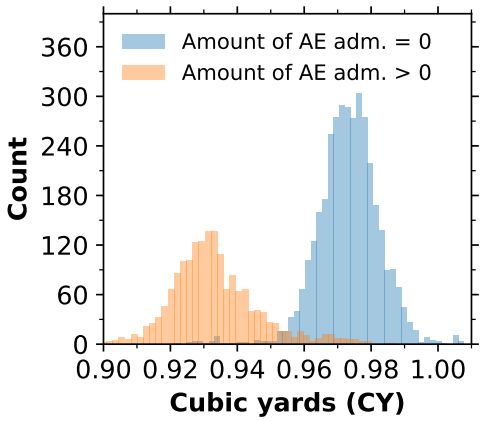

Figure 4: Histogram of calculated volumes of mixtures (V_m) in our industrial dataset using constituent densities in Table 4 and Eq. 19. Units are in CY (~ 0.76 m^3).

$$V_{agg} = \frac{z_1/\rho_1 + z_2/\rho_2}{V_{final}} \tag{22}$$

$$0.65 \leq V_{agg} \leq 0.75 \tag{23}$$

where z_j and ρ_j are the quantity and density of the jth constituent (see the constituent label in Table 4), respectively; V_{agg} is the volume ratio of aggregate (including both fine and coarse aggregates) in the final concrete mix.

3.3.2. Optimization algorithm and objective function

Here, we have considered two optimization objectives for designing a concrete mixture, minimizing the climate impact ($f_g(\mathbf{z})$, Eq. 11), and cost ($f_g(\mathbf{z})$, Eq. 12) and two settings, with and without constraints on the air-entraining admixture (Eq. 20), resulting in four single-objective optimization problems. We used the differential evolution (DE) algorithm, a heuristic optimization algorithm developed by Storn and Price [52], to find the optimal solutions (i.e., mix proportions with minimal climate impact or cost) subject to the bounds and constraints in Section 3.3.1. We use the DE implementation available in the SciPy Python package [53]. More details on the DE algorithm and a summary of each single-objective optimization scheme (minimizing climate impact or cost) are given in Appendix. In each case, the algorithm was

Table 5: Ratio constraints used in the optimization procedure. In all cases, the denominator is the total cement, fly ash, slag and silica fume. These bounds are selected based on the ranges of the ratios in the original dataset (see Table 1).

Parameter	**Expression**	**Lower**	**Upper**
Total supplementary cementitious material ratio (R_{SCM})	$\frac{z_5 + z_6 + z_7}{z_4 + z_5 + z_6 + z_7}$	0	0.6
Fly ash ratio (R_{FA})	$\frac{z_5}{z_4 + z_5 + z_6 + z_7}$	0	0.4
Slag ratio (R_{BFS})	$\frac{z_6}{z_4 + z_5 + z_6 + z_7}$	0	0.6
Silica fume ratio (R_{SF})	$\frac{z_7}{z_4 + z_5 + z_6 + z_7}$	0	0.1
w/cm (R_{WCM})	$\frac{z_3}{z_4 + z_5 + z_6 + z_7}$	0.2	0.6

run 50 times for each target strength using the Sobol population initialization method, generating an ensemble of optimal solutions (local minima).

Bi-objective optimization. We then performed bi-objective optimization, which aims to jointly minimize both climate impact and cost. Following the methods in ref. [54], we normalize each of the single objective functions using Eqs. 24 and 25, where $\mathbf{z}_c^*$ and $\mathbf{z}_g^*$ are the concrete mix formula which minimizes f_c (cost) and f_g (climate impact), respectively.

$$f_c^{norm}(\mathbf{z}) = \frac{f_c(\mathbf{z})}{f_c(\mathbf{z}_c^*)} \tag{24}$$

$$f_g^{norm}(\mathbf{z}) = \frac{f_g(\mathbf{z})}{f_g(\mathbf{z}_g^*)} \tag{25}$$

There are several classical methods for multi-objective optimization problems, including ϵ-constraint, goal attainment, and weighted sum. Here, we adopted the weighted sum method, which involves converting the multi-objective problem into a weighted sum of all single objectives and is among the simplest and most popular to implement. The new function to be minimized (F) for our bi-objective problem is given in Eq. 26. In this form, we alter the values of the weighting factor w in the range $[0, 1]$ in order to vary the prioritization of one objective over another. As a result, we will be able

to understand the trade-offs between the two objectives (i.e., minimizing cost and climate impact).

$$F = w \cdot f_g^{norm}(\mathbf{z}) + (1 - w) \cdot f_c^{norm}(\mathbf{z}) \tag{26}$$

4. Results and Discussion

4.1. Strength prediction based on GP model

We examined the performance of the novel amortized GP model (as given in Section 3.1) in predicting concrete strength. Fig. 5(a) and 5(c) show the strength trajectories for two example concrete mixtures (from the 20% testing set not exposed during model training) predicted using the GP model, in comparison with the corresponding experimental data. It is clear that the GP model gives reasonable strength predictions and captures the general trend of strength evolution (i.e., growth of strength with time at a decreasing rate of growth). Fig. 5(b) and 5(d) show the updated prediction trajectories after informing the model an early-age measurement for the two concrete mixes in Fig. 5(a) and 5(c), respectively. Comparison with the experimental data shows that the early-age inference improves the prediction accuracy of the later-age strength for both cases and reduces the uncertainty of predictions, as also shown previously [21].

Next, we evaluate the GP model's ability to speed up experimentation by using the 28-day strength predicted from the posterior estimate of the model conditioned on an earlier time point as surrogate data to shorten experiment times. As a proof-of-principal, we consider the mixes in the test set which have measurements at 14 and 28 days. This is a comparatively small number of samples, therefore we consider four additional train-test splits for the analysis (resulting dataset has an average of 74 samples per split). All results presented here are on the testing data, i.e. data not used to learn the model parameters. We propose an early stopping criterion for the experiment based on the prediction of 14-day strength, i.e., if our prediction at baseline for 14-day strength is close to the observation at 14-days, accept the posterior prediction for 28-day strength and terminate the experiment, else continue the experiment until 28-days. Setting a threshold of 20% error, we achieve a 28-day error of 475 $\pm$ 32 psi or 3.3 $\pm$ 0.2 MPa (5.3 $\pm$ 0.4%) for the mixes that meet the criteria, which translates to stopping 90 $\pm$ 4% of experiments early, reducing experiment time by half for those mixes. In comparison, the points that don't meet the early stopping criteria have a 28-day error of 801 $\pm$ 262 psi or 5.5 $\pm$ 1.8 MPa (10.0 $\pm$ 2.3%). This analysis shows that the GP model with early-age inference may be able to replace the need for 28-day (or later age) strength measurements, significantly decreasing the experimental time frame.

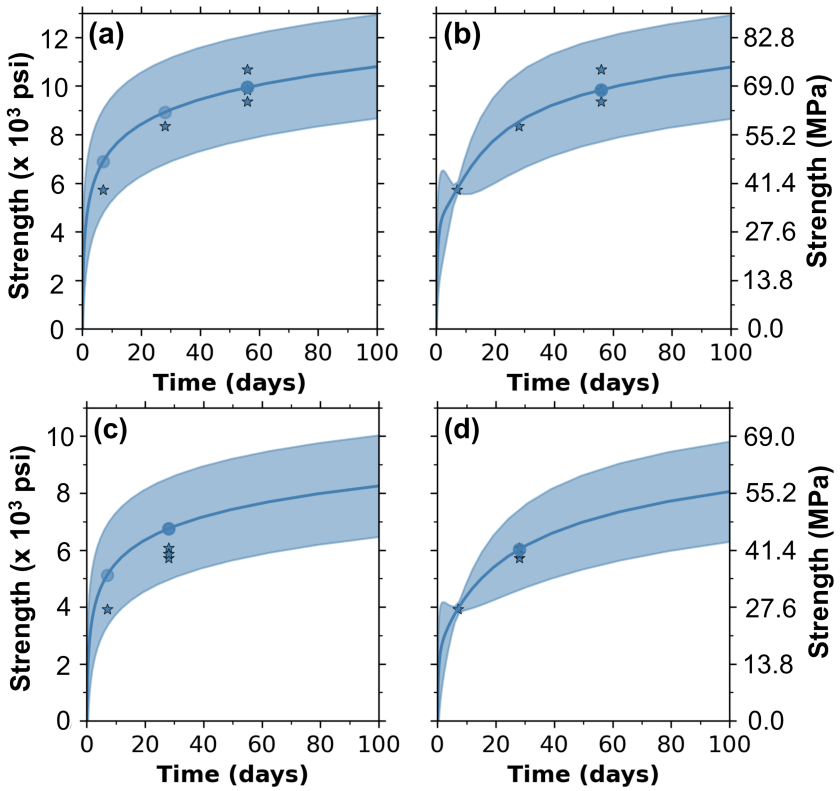

Figure 5: (a) and (c) show the predicted strength trajectories (1000 psi = 6.9 MPa) of two concrete mixes (in the 20% testing set) from the amortized GP model, in comparison with the corresponding experimental data at specific ages. (b) and (d) show the impact of early-age inference on the predicted strength trajectories of the two concrete mixes in (a) and (c), respectively. Experimental data are given by the stars, while the circles and lines represent the average predicted strength at given ages and strength trajectories, respectively. The blue shaded areas represent 95% confidence interval.

Fig. 6 compares the performance of the GP model in predicting concrete strength at all ages for the 20% testing set with that of typical RF and ANN models trained using the same 80% data for training and validation. Details on the training of the RF and ANN models are given in the Supplementary Material. The amortized GP model is seen to give an R^2 value, RMSE and MAPE of ∼0.88, ∼909 psi (∼6.3 MPa), and ∼10.8%, respectively, which are comparable to those obtained from the RF and ANN models (R^2 value, RMSE and MAPE of ∼0.88-0.89, ∼876-932 psi (∼6.0-6.4 MPa), and ∼10.3-10.4%, respectively). The prediction performance of the models presented here is reasonably good given the inherent uncertainty and complexity of the industry data set as discussed earlier (Section 2). The R^2 value achieved here for the 28-day strength prediction only is about 0.83, higher than those reported by Young et al. [6] and DeRousseau et al. [11], where R^2 values of ∼0.54-0.60 and ∼0.25-0.51 were achieved for predicting the 28-day strength of industrial concrete using different ML models (including RF and ANN), respectively. Overall, the results in Figs. 5 and 6 suggest that our GP model works reasonably well in predicting strength and strength trajectories of industrial concrete mixes.

4.2. Single objective optimization

The optimized costs and climate impacts as a function of 28-day design strength from the single-objective optimization are presented in Fig. 7(a) and 7(b), respectively. Each violin shape in Fig. 7 represents a distribution of objective values achieved over 50 independent algorithm runs, with the median of the data given by the circle in the middle. The scattering of the results, particularly notable for the case of minimizing climate impact at a target strength of 12000-13000 psi (82.8-89.7 MPa), suggests that the optimization is challenging and contains many local minima.

It is clear from Fig. 7 that there is an overall trend of increasing cost and climate impact for the optimized concrete mixes as the target 28-day strength increases. This overall trend is consistent with previous studies [55, 6, 28], which also show that the cost and climate impact of concrete mix is generally positively correlated with its strength. Fig. 7 also reveals that this relationship is nonlinear: the increase of cost and climate impact per 1000 psi (6.9 MPa) increase in target strength (i.e., the slope of the data) is higher at a higher target strength. For instance, the slope of cost over the target strength of 6000-11000 psi (41.4-75.9 MPa) is about 1.6\$/CY/1000 psi (\$0.3/m^3/MPa,

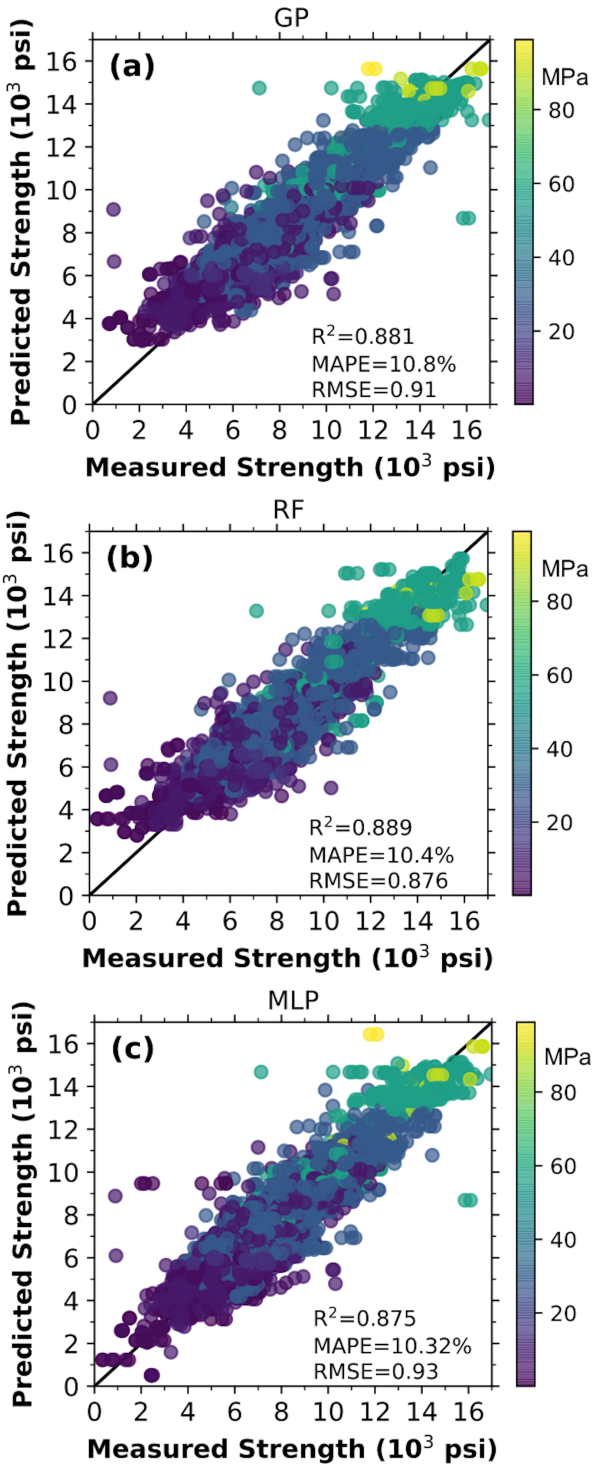

Figure 6: Comparison of measured concrete compressive strength with the predicted strength at different ages from the (a) amortized GP model, (b) RF model, and (c) ANN model. Selected error statistics are given in the figure. The RF and ANN models were trained using the same 80% training data with a five-fold cross validation (see more details on the RF and ANN models in Supplementary Material). The solid black line represent the line of equality.

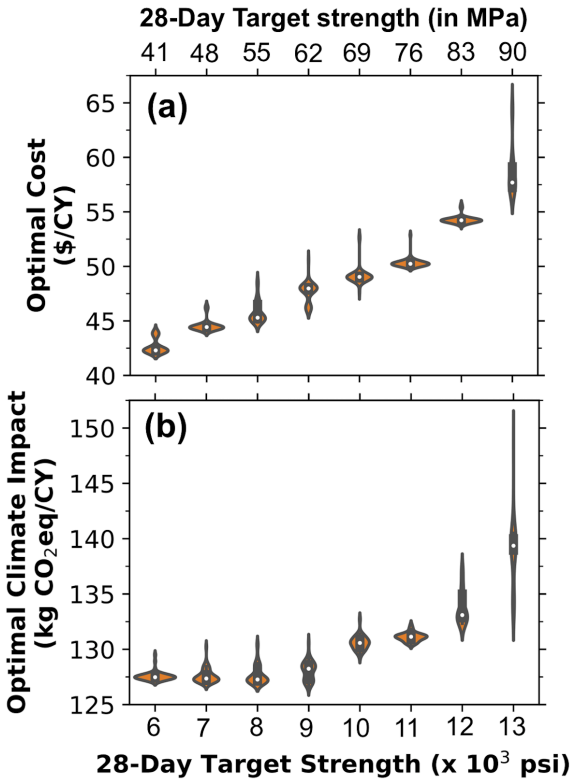

Figure 7: Evolution of the (a) cost and (b) climate impact of the optimized mixes produced by cost and climate impact minimization, respectively, as a function of 28-day target strength. Each violin distribution is based on results from 50 independent algorithm runs, with median value given by the open circle. 1000 psi = 6.9 MPa. 1 cubic yard (CY) = 0.76 m^3.

Fig. 7(a)), which is significantly lower than that over the range of 11000-13000 psi = 75.9-89.7 MPa (\$3.8/CY/1000 psi = \$0.7/m^3/MPa). For the climate impact data in Fig. 7(b), the slope over the design strength of 11000-13000 psi = 75.9-89.7 MPa (∼3.8 kg CO_2-eq/CY/1000 psi = ∼0.7 kg CO_2-eq/m^3/MPa) is also considerably higher than that over 4000-11000 psi (∼ 0.7 kg CO_2-eq/CY/1000 psi = ∼0.1 kg CO_2-eq/m^3/MPa). Fig. 7 appears to suggest the existence of change points of design strength (e.g., 12000 psi = 82.8 MPa) in terms of reducing cost and climate impact while increasing strength. Nevertheless, for a given task, one must consider that a higher strength can reduce the size of a concrete beam or column (hence the volume of concrete materials) needed.

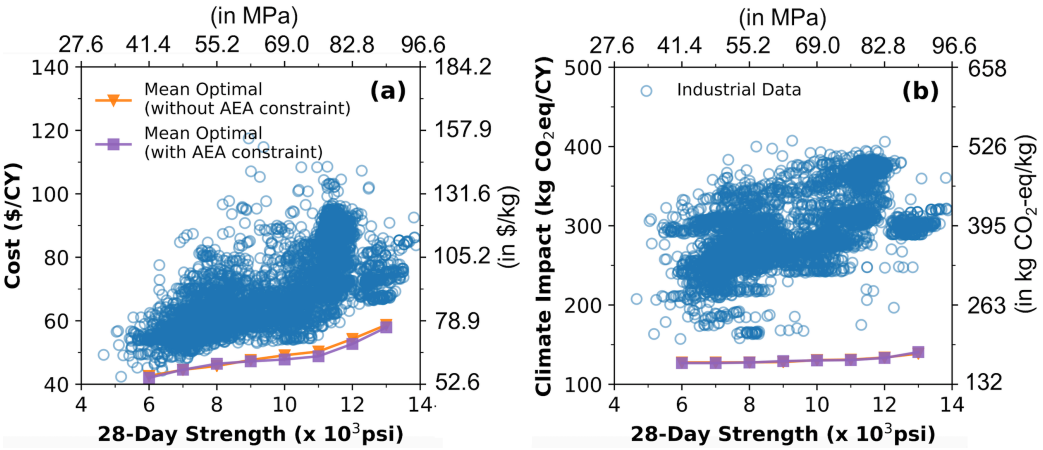

Figure 8: Evolution of (a) cost and (b) climate impact of the optimized concrete mixes (generated from the corresponding single-objective optimization) as a function of the 28-day target strength in psi (1000 psi =6.9 MPa). The average optimization results based on 50 independent production runs for two schemes (with and without an imposed AEA constraint, see Section 3.3.1) are shown in the figure (orange triangles and purple squares) in comparison with cost and climate impact of the industrial concrete mixes (unfilled blue circles). 1 cubic yard (CY) = 0.76 m^3.

To illustrate the potential benefits of these optimizations, we compare the cost and climate impact of the observed concrete mixes in our industrial dataset (calculated using Eqs. 12 and 11, respectively) with those of the optimized concrete mixes in Fig. 8(a) and Fig. 8(b), respectively. A comparison of the two schemes (with or without an imposed AEA constraint, as described in Section 3.3.1) shows that the imposed AEA constraint does not alter the overall trends in Fig. 8 yet slightly decreases the cost at 10,000-12,000 psi (69.0-82.8 MPa). We note that, for the industry data, only mixtures conforming to the bounds and constraints imposed for optimization (see Tables 4 and 5) are shown in Fig. 8 for a fair comparison. This comparison demonstrates that the cost and climate impact of the optimized concrete mixes are generally considerably lower than those of the actual mix designs used by the industry. Calculations show that, on average, the cost and climate impact of the industry mixes are ~\$68/CY (~\$89/m^3) and ~304 kg CO_2-eq/CY (~400 kg CO_2-eq/m^3), respectively. These large gaps highlight the potential economic and environmental benefits of data-driven concrete mix design.

To better understand whether the optimization algorithm is producing feasible concrete mix designs, we examine the quantity of each constituent

of the optimized mixes as a function of the target 28-day design strength. Fig. 9 compares the actual constituent quantities (blue circles) from our industry data with the results from four single-objective optimization schemes: minimizing (i) cost and (ii) climate impact without imposing a constraint on AEA, and minimizing (iii) cost and (iv) climate impact considering the AEA constraint (see Section 3.3.1). The AEA constraint in schemes (iii) and (iv) impose a minimal AEA content ($z_{11}/(z_4/100) \geq 0.39$) and 7% entrained air. The average values based on 50 runs along with the standard deviation are given in Fig. 9, while Fig. S4 of the Appendix illustrates the typical distributions of quantities from the 50 runs for schemes (i) and (ii) and a design strength of 10000 psi (69 MPa).

The overall trends in Fig. 9 are largely consistent with expectation or domain knowledge. In all four cases, the optimized mixtures use less cement and more FA, as the former is more costly and carbon-intensive. In the case of minimizing cost (scheme (i)), the algorithm tends to generally increase the use of FA (Fig. 9(f)) and HRWR admixture (Fig. 9(h)) while reducing the quantity of cement (Fig. 9(d)) and other types of organic admixtures (Fig. 9(i)-(l)), compared with the industry data. The reduction in cement usage and organic admixtures (other than the HRWR admixture) makes sense given that cement is the most expensive constituent in concrete (see the cost distribution of all concrete constituents for the industry mixes in Fig. S5 of Appendix), while the latter has a less direct impact on 28-day strength. The FA replacement ratios for the optimized mixes are about 0.4 ($\sim$200/(250+200+50)= $\sim$0.4) for most of the target strengths (see the evolution of the FA ratio in Fig. S6, which are close to the upper limit set for FA (0.4, as seen in Table 5). In contrast, the predicted BFS replacement ratios ($\sim$50/(250+200+50)=$\sim$0.1) are significantly lower than the set limit (0.6, Table 5). This difference is mainly attributed to the lower assigned cost of FA ($0.055/kg) than BFS ($0.11/kg), leading to the prioritization of FA usage.

Furthermore, the overall SCM replacement ratio stay at about 0.5, as seen in Fig. S6. At higher design strengths ($>$ $\sim$11,000 psi (75.9 MPa)), SF quantity is increased at the expense of FA. This observation can be explained by the domain knowledge, where numerous studies have shown that high FA replacement ratios tend to lower the 28-day compressive strength of concrete [56, 57, 58] while small additions of SF improve 28-day concrete strength [36, 35]. At the same time, we also see an overall reduction of water (and hence w/cm ratio, Fig. 9c) in the optimized mixes, which is known to in-

crease concrete strength [34, 35]. On the other hand, the reduction of w/cm ratio and increase of SF content are known to decrease concrete workability [35] (critical to the proper placement of concrete), which can be resolved by increasing the quantity of HRWR admixture, as has been captured by our optimization algorithm (Fig. 9(h)). This is encouraging given that workability (e.g., slump) has not been used in training the GP model nor during the implementation of the optimization framework. Furthermore, the predicted increase for constituents with the highest unit price (i.e., \$0.397/kg for SF; \$2.928/kg for HRWR admixture) at high design strengths in the case of minimizing cost suggests that the model is generally doing its job (i.e., capturing the key factors that improve strength even at the expense of increasing cost). Finally, the predicted quantities of the coarse and fine aggregates in the optimized mixes fall within the range of the industry records. It appears that the quantity of coarse aggregate tends to lean towards the lower end of the industry data range, while the quantity of fine aggregate tends to lean towards the upper end of the industry data range (also evident from Fig. S4a-b).

In the case of minimizing climate impact (scheme (ii)), the optimization algorithm is seen to minimize the use of cement (i.e., it remains at the lower bound of 200 lb/CY ($\sim$340 kg/m^3) for all design strengths, Fig. 9(d)) while maximizing the use of SCMs (i.e., the replacement ratio remains at the upper bound of 0.6 at all design strengths, Figs. 9(e)-(g) and Fig. S6). This is attributed to the fact that the assigned climate impact of cement (1.072 kg CO_2-eq/kg) is $\sim$6-47 times higher than that of the SCMs ($\sim$0.023-0.166 kg CO_2-eq/kg). Among the three SCMs, the algorithm is seen to drive up the replacement of cement with FA and SF toward their upper bounds in Table 5 (0.4 and 0.1, respectively), which is attributed to their lower assigned climate impact ($\sim$0.023 kg CO_2-eq/kg) compared with that assigned to BFS ($\sim$0.166 kg CO_2-eq/kg). Given that the predicted quantities of cement and SCMs do not vary significantly at increasing 28-day target strength, this increased performance requirement is mainly achieved via decreasing water content (and hence w/cm ratio), as evidenced by Fig. 9(c) (and Fig. S6(e)). The reduction in workability due to decreasing w/cm is then mitigated by increasing the usage of HRWR admixture (see Fig. 9(h)).

For schemes (iii) and (iv), where a constraint has been imposed on AEA during optimization, the general trends of evolution are largely consistent with schemes (i) and (ii), respectively. A major difference is seen in Fig. 9(c), where we see generally lower w/cm for schemes (iii) and (iv) than schemes (i) and (ii), respectively, at a given target strength. This is because the former

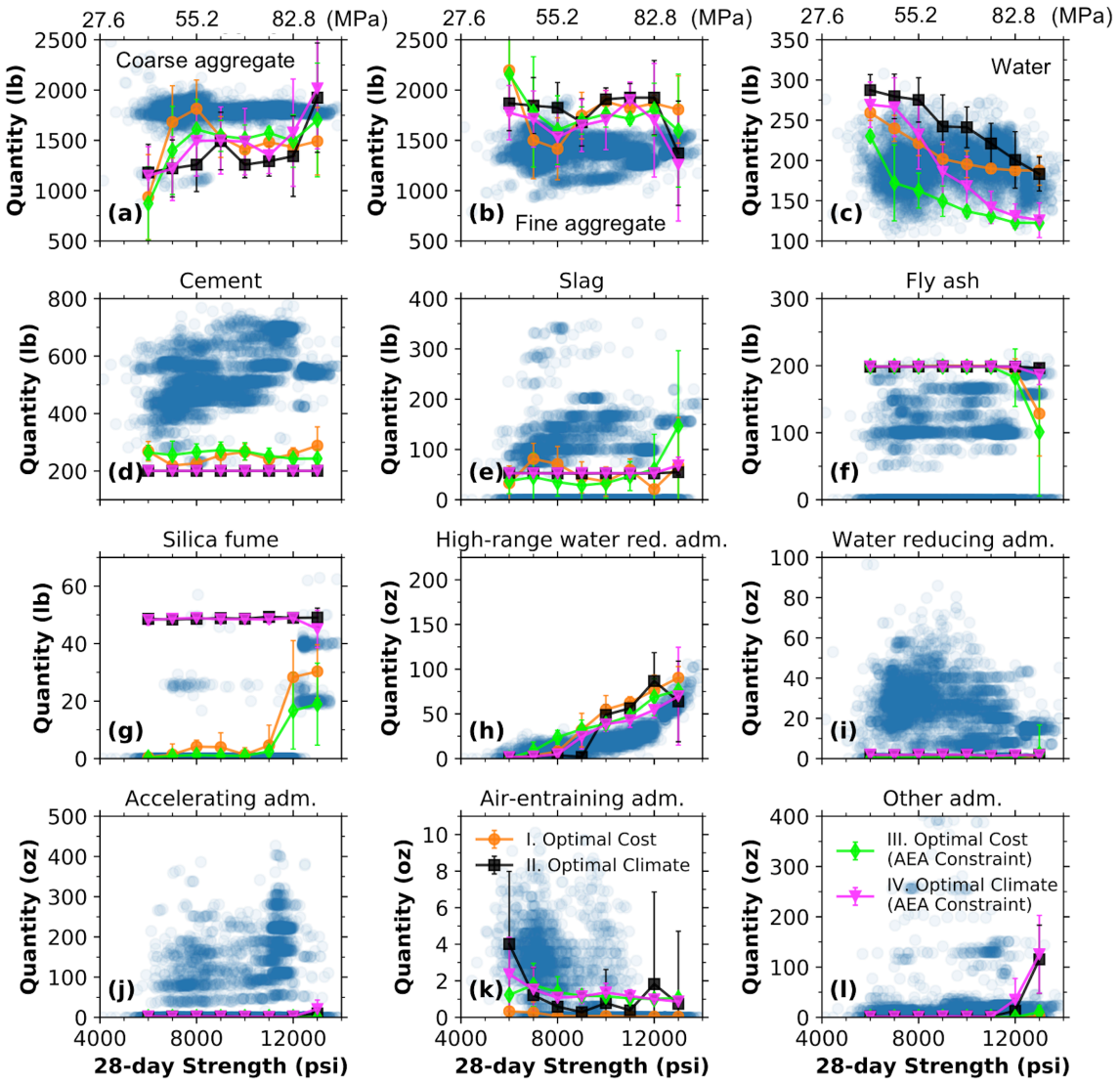

Figure 9: Evolution of the constituent quantities (as labelled in each figure: 1 lb = 0.45 kg; 1 oz = 0.028 kg) in the optimized concrete mixes as a function of 28-day design strength in psi (1000 psi = 6.9 MPa). Each figure contains four evolution curves, which are based on results from four single-objective optimization scenarios: (i) cost and (ii) climate impact minimization without constraint imposed on air-entraining admixture (AEA), and (iii) cost and (iv) climate impact minimization with AEA constraint. Each constituent quantity in the figures is an average value based on 50 independent production runs, with the error bars representing one standard deviation. The constituent quantities of the industry mix designs in our database are given in the figures (blue circles) for comparison.

two schemes generate concrete mixes with more entrained air (7% vs 3%) due to presence of AEA (the assumption made based on Fig. 4 and Fig. S3 of Appendix, as explained in Section 3.3.1), leading to reductions in strength (as entrained air negatively impact strength [37]). This strength reduction is then compensated by decreasing w/cm ratio, which is known to increase strength [34, 35].

Next, we examine how the optimization results change as the unit price of the SCM increases, which is a feasible future scenario given that the annually produced high-quality BFSs and FAs are already almost fully utilized [9]. Our industry data show that ∼20% of the mixes do not contain any SCMs and that the average SCM replacement ratio used in this industry data set is ∼16%, which is significantly lower than the optimized mix designs for all four cases of optimizations shown in Fig. 9 (average SCM replacement ratios of ∼45-60%). This large discrepancy may be partially attributed to the lack of sufficient locally-accessible high-quality SCMs in reality, although other factors need to be considered as well, including reduced early-age strength often associated with high SCM ratios [10, 56, 57, 58]. Specifically, we have studied the impact of three scenarios with an increased unit price for (1) FA, (2) BFSs, and (3) both BFSs and FAs, from the baseline level (see Fig. 3) on the cost of the optimized concrete mixes. The results based on 50 independent production runs are presented in Fig. 10, which shows the expected increase of optimal cost with increasing 28-day target strength for all scenarios. We also see that the cost of the optimized mixes generally increases with the increasing unit price of SCMs, as expected. However, comparing Scenarios 1 and 2 with the baseline reveals considerably larger increases in cost for the optimized mixes when the unit price increase ($0.55/kg) is applied on FA (Scenario 2) as opposed to BFS (Scenario 1). This is because the optimized mixes in the baseline scenario contain more FA than BFS and hence are more sensitive to the unit price increase of the former.

4.3. Bi-objective Optimization

Although the single objective optimizations in the previous section have generally captured important domain knowledge in concrete mix design, multi-objective optimization is more useful in understanding the trade-offs between different objectives. This is likely to be the case for concrete mix design in the future concrete industry, where one needs to consider both cost and climate impact at the same time. Following a weighted sum method

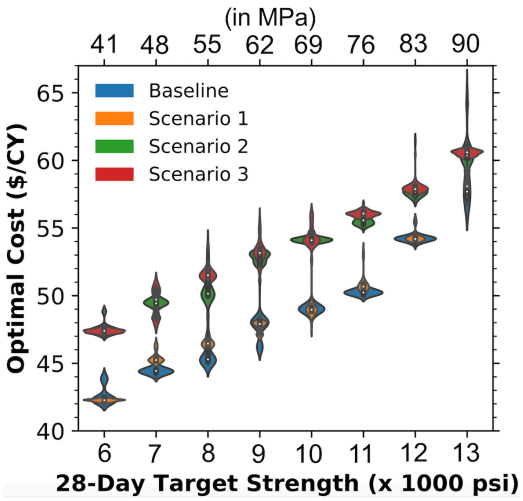

Figure 10: Impact of increasing the unit price of BFS (Scenario 1), FA (Scenario 2), and both BFS and FA (Scenario 3) from the baseline scenario on the cost of the optimized concrete mixes (minimizing cost) at different 28-day target strengths. Details on the different scenarios are given Fig. 3. Each violin plot shows the distribution of costs based on 50 independent production runs with the open circle representing the median value. 1000 psi =6.9 MPa. 1 CY = $\sim$ 0.76 m^3.

described in Section 3.3.2, we have minimized both the cost and climate impact of concrete mixes with a weighting factor w varying from 0 to 1 (at an increment of 0.1) for the objective function (Eq. 26) with respect to the bounds and constraints specified in Section 3.3.1.

The results are presented in Fig. 11, which includes 50 independent optimization runs at each weighting factor and each target strength. This gives a total of 550 points (each corresponding to a local minima) for each target strength. A weighting factor of 1 (ligher colors in Fig. 11) and 0 (darker colors in Fig. 11) represents single-objective optimization that aims to minimize climate impact and cost, respectively. Overall, we see a general increase in cost and climate impact for the optimized mixes at increasing target strength, which is consistent with expectation. We then determine the Pareto front at each target strength with respect to the weighing factor (indicated by the lines in Fig. 11) by connecting the optimal solutions (the lowest and leftmost point at each weighting factor), which reveals the existence of a trade-off between cost and climate impact for the optimal solutions. Most of these lines (except for the case of 7,000 psi = 48.3 MPa) can be approximated with

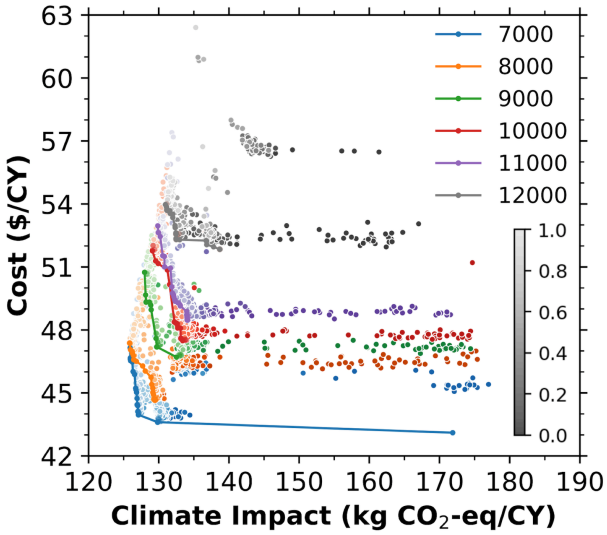

Figure 11: Pareto fronts for the bi-objective minimization of climate impact and cost (using the Eq. 16) for 28-day design strengths of 7,000, 8,000, 9,000, 10,000, 11,000, and 12,000 psi (48.3, 55.2, 62.1, 69.0, 75.9, and 82.8 MPa). For each target strength, there are 550 points, with 50 points at each weighting factor (each point corresponds to a local minimal solution). At each target strength, the points are color-coded from dark to light as the weighting factor increases from 0 to 1, at an increment of 0.1. Each line in the figure gives the optimal solutions among the 550 algorithm runs. 1 cubic yard (CY) = $\sim$ 0.76 m^3.

linear equations with a slope of –0.5-1\$/kg CO_2-eq (i.e., a cost increase of 0.5-1\$ for every kg CO_2-eq saved).

Furthermore, we note that the climate impact of mixes optimized based on cost only can have large variance. For example, considering a design strength of 9,000 psi (62.1 MPa) and a weighting factor 0 (minimizing cost only), the resulting range of climate impact is approximately 135-175 kg CO_2-eq/CY over 50 runs of the optimization algorithm ($\sim$30% variation). This means that, without many independent runs, one may produce mixes with unnecessarily large climate impact. In contrast, the bi-objective optimization, even with a weighing factor of 0.1 assigned to climate impact, significantly lowers the spread of climate impact for all the generated mixes, approximately 135-140 kg CO_2-eq/CY with minimal compromise on cost (see Fig. S7 of the Appendix for a direction comparison of the spread from the 50 runs for the weighting factor of 0 and 0.1).

Table 6 shows the optimal mix designs for a target 28-day strength of

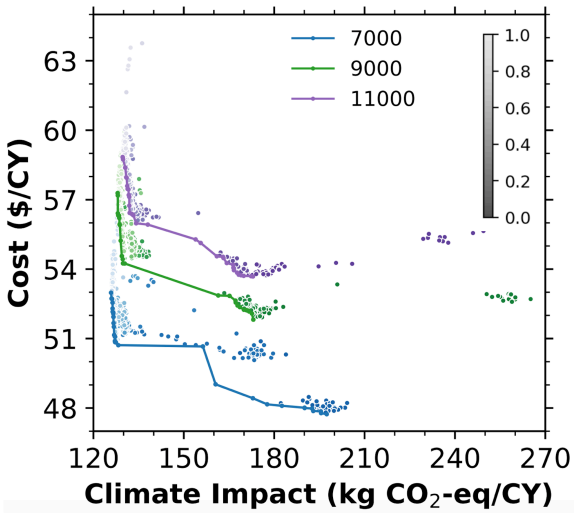

Figure 12: Pareto fronts for the bi-objective minimization of climate impact and cost (based on cost scenario 3 in Fig. 3, where both the unit price of blast-furnace slag (BFS) and fly ash (FA) increase by \$0.055/kg from the baseline) for 28-day design strengths of 7,000, 9,000, and 11,000 psi (48.3, 62.1, and 75.9 MPa). For each target strength, there are 550 points, with 50 points at each weighting factor (each point corresponds to a local minimal solution). At each target strength, the points are color-coded from dark to light as the weighting factor increases from 0 to 1, at an increment of 0.1. Each line in the figure gives the optimal solutions among the 550 algorithm runs. 1 cubic yard (CY) = $\sim$ 0.76 m^3.

7,000, 9,000, and 11,000 psi (48.3, 62.1 and 75.9 MPa), identified from the bi-objective optimization (Fig. 11), with a weighting factor of 0.5. The corresponding mix designs from the single-objective optimizations are also given in Table 6. We have compared the cost and climate impact of the three mixes from the bi-objective optimization with those of the industrial mixes with similar measured 28-day strength (6,500-7,500, 8,500-9,500, and 10,500-11,500 psi, respectively). The comparison show that the optimized mixes from our computational framework are about 28-35% lower in cost and 56-57% lower in climate impact. We note that the mixes presented in Table 6 are provided as examples of possible optimal solutions from the optimization framework proposed here for the given conditions (e.g., the cost and climate impact factors in Tables 3 and 2). It is important to recognize that the cost and climate impact factors for individual constituents in Tables 2 and 3 may evolve with time, source and region, which, upon change, will leads to different optimal solutions.

Table 6: Optimal mix designs obtained from the bi-objective optimization (minimizing both climate impact and cost) for target 28-day strengths of 7,000, 9,000, and 11,000 psi (48.3, 62.1 and 75.9 MPa), in comparison with the optimal design from single objective optimization (minimizing either climate impact or cost). The optimal solutions for the bi-objective optimization are identified with a weighting factor of 0.5, as seen in Fig. 11. The quantities are based on generating 1 cubic yard (CY) of concrete (1 CY = ∼0.76 m^3). 1 lb = 0.45 kg; 1 oz = 0.028 kg.

j	Constituent or ratio	Min. cost			Min. climate impact			Bi-objective (w=0.5)		
		7000	9000	11000	7000	9000	11000	7000	9000	11000
1	Coarse agg., lb	1834	1457	1507	937	1249	1401	715	1893	1483
2	Fine agg., lb	1330	1840	1796	2027	1828	1886	2160	1230	1781
3	Water, lb	228	174	172	299	261	172	285	192	135
4	Cement, lb	200	227	203	200	200	200	200	200	200
5	Fly ash, lb	200	200	199	200	200	199	200	200	200
6	Slag, lb	100	72	98	51	51	51	72	83	99
7	Silica fume, lb	0	0	0	49	49	50	29	17	1
8	HRWR adm., oz	0.0	41.5	67.4	1.0	0.7	45.1	0.0	12.7	53.9
9	Water reducing adm., oz	0.0	0.3	0.5	0.3	3.1	1.5	0.4	0.3	0.1
10	Acc. adm., oz	0.1	0.1	0.3	1.4	4.7	0.2	0.2	1.2	1.1
11	Air-ent. adm., oz	0.8	1.0	0.8	1.4	0.9	0.8	0.8	0.8	0.9
12	Other adm, oz	0.0	0.0	0.0	0.1	0.5	0.1	0.1	0.2	0.2
	w/cm	0.46	0.35	0.34	0.60	0.52	0.34	0.57	0.38	0.27
	Slag ratio	0.2	0.14	0.2	0.1	0.1	0.1	0.14	0.17	0.2
	Fly ash ratio	0.4	0.4	0.4	0.4	0.4	0.4	0.4	0.4	0.4
	Silica fume ratio	0	0	0	0.1	0.1	0.1	0.06	0.03	0
	SCM ratio	0.6	0.55	0.59	0.6	0.6	0.6	0.6	0.6	0.6
	Agg. ratio	0.7	0.73	0.73	0.65	0.68	0.72	0.65	0.71	0.74
	Cost	44	48	50	48	49	54	44	47	49
	Climate impact	131	145	136	127	127	130	127	130	134

Fig. 12 illustrates the results of bi-objective optimization for target design strengths of 7,000, 9,000, and 11,000 psi (48.3, 62.1, and 75.9 MPa), considering the cost scenario #3 in Fig. 3, where both the unit price of BFS and FA increases by \$0.055/kg from the baseline scenario. The Pareto fronts in Fig. 12 reveal clear trade-off between cost and climate impact. As a consequence of the increased unit price of BFS and FA, the cost of the optimal solutions for a given target strength is generally higher than those in Fig. 11 based on the baseline cost scenario. It is also clear from Fig. 12 that the optimized solutions exhibit higher climate impact than those in Fig. 11 at a low weighting factor (e.g., w=0; minimizing cost only). This observation can be attributed to a reduction in BFS and FA replacement due to their increased unit price, resulting in higher OPC content and consequently higher climate impact. This is clearly seen for the cost minimization (w=0) results in Table 7, where the optimal mixtures exhibit a 30-80% increase in cement quantity and a 20-50% increase in climate impact than those in Table 6. Additionally, it is interesting to note that bi-objective (w=0.5) optimal solution in Table 7 exhibit higher costs (as expected), yet slightly lower climate impact (for design strength of 9,000 and 11,000 psi) than the corresponding mix in Table 6.

Furthermore, the Pareto fronts (connected lines) in Figure 12 exhibit two distinct regions with different slopes for linear regression: (i) a slope of -$\sim$1\$/kg CO_2-eq (i.e., a cost increase of $\sim$1\$ for every kg CO_2-eq saved) when the weighing factor is high (more emphasis on minimizing climate impact), and (ii) a slope of -$\sim$0.05\$/kg CO_2-eq (i.e., a cost increase of $\sim$0.05\$ for every kg CO_2-eq saved) when the weighing factor is low (higher weighting on cost minimization).

4.4. Prediction of early-age strength development

Given that a key issue identified with using a high content of SCMs is the slow development of early-age strength [10, 56, 57, 58], we use our GP model to estimate the strength trajectories for the optimal concrete mix design identified from the bi-objective optimization based on the baseline cost scenario (i.e., the mix designs given in Table 6). The predicted strength trajectories for the target 28-day strengths of 7,000, 9,000, and 11,000 psi (48.3, 62.1 and 75.9 MPa, respectively) are presented in Fig. 13, which shows that the predicted 3-day strengths are $\sim$3,000 (20.7), $\sim$4,800 (33.1), and $\sim$7,600 (52.4) psi (MPa), respectively. These are considerably higher than the minimum strength specified in some standards for supporting formwork

Table 7: Optimal mix designs obtained from the bi-objective optimization (minimizing both climate impact and cost) for target 28-day strengths of 7,000, 9,000, and 11,000 psi (48.3, 62.1 and 75.9 MPa) based on cost scenario #3 in Fig. 3. The optimal design generated from single objective optimization (minimizing either climate impact or cost) are also shown for comparisons. The optimal solutions for the bi-objective optimization are identified with a weighting factor of 0.5, as seen in Fig. 11. The quantities are based on generating 1 cubic yard (CY) of concrete (1 CY = ∼0.76 m^3). 1 lb = 0.45 kg; 1 oz = 0.028 kg.

j	Constituent or ratio	Min. cost			Min. climate impact			Bi-objective (w=0.5)		
		7000	9000	11000	7000	9000	11000	7000	9000	11000
1	Coarse agg., lb	709	1850	1628	793	1984	1377	736	1872	1341
2	Fine agg., lb	2472	1383	1674	2066	1195	1892	2135	1242	1953
3	Water, lb	175	154	126	286	173	137	283	195	125
4	Cement, lb	357	303	308	200	200	200	201	200	200
5	Fly ash, lb	144	196	188	200	200	200	200	199	200
6	Slag, lb	0	1	0	51	51	51	72	77	82
7	Silica fume, lb	0	1	6	50	49	49	29	23	19
8	HRWR adm., oz	0.1	23.1	38.0	0.1	3.7	35.7	0.1	9.6	39.7
9	Water reducing adm., oz	0.3	0.3	0.1	0.4	0.1	0.2	0.3	0.2	0.3
10	Acc. adm., oz	0.4	0.6	0.1	0.4	1.0	0.3	0.3	0.1	0.6
11	Air-ent. adm., oz	1.4	1.2	1.2	1.3	0.9	1.0	0.9	0.8	0.8
12	Other adm, oz	0.0	0.8	0.2	0.2	0.6	0.1	0.2	0.8	0.2
	w/cm	0.35	0.31	0.25	0.57	0.35	0.27	0.57	0.39	0.25
	Slag ratio	0	0	0	0.1	0.1	0.1	0.14	0.15	0.16
	Fly ash ratio	0.29	0.39	0.37	0.4	0.4	0.4	0.4	0.4	0.4
	Silica fume ratio	0	0	0.01	0.1	0.1	0.1	0.06	0.05	0.04
	SCM ratio	0.29	0.4	0.39	0.6	0.6	0.6	0.6	0.6	0.6
	Agg. ratio	0.72	0.73	0.75	0.65	0.72	0.74	0.65	0.71	0.75
	Cost	48	52	54	53	57	59	51	55	56
	Climate impact	199	175	178	126	128	130	127	129	132

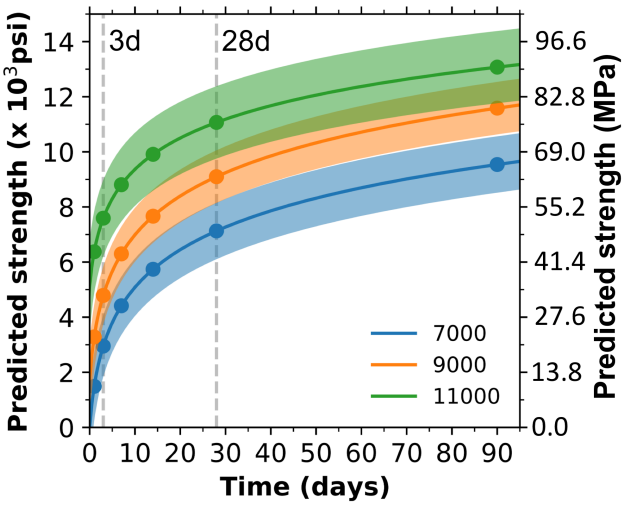

Figure 13: Predicted strength trajectories from our GP model for the three optimal concrete mixes based on the baseline cost scenario (see Table 6) identified from bi-objective optimization (minimizing both climate impact and cost) for a 28-day target strength of 7000, 9000, and 11000 psi (48.3, 62.1 and 75.9 MPa). The solid lines represent the mean predictions while shadow regions represent 95% confidence level.

removal, e.g., 5-8 MPa (725-1,160 psi) [59, 60] and 10 MPa (1,450 psi) [61]. The 2-day/28-day strength ratios are ∼33%, ∼46% and ∼64%, respectively, which correspond to medium, medium, and rapid strength development of concrete, respectively, according to standard EN 206-1:2000 [62]. Overall, the predicted strength trajectories for the optimal mixes from bi-objective optimization are seen to be reasonable. However, we have also calculated the 3-day (and 28-day) strengths of these optimized mixes using the RF and MPL models (Figs. 6(b) and (c)), which are 700-3200 (4500-6200), 2700-5100 (6100-7700), and 4700-5300 (8200-8400) psi, respectively. These strength values are generally lower than those from the GP model. Future research is needed to experimentally verify the strength trajectories of the mixes in Tables 6 and 7. These additional data can then be used to improve the performance of the GP model and the optimization framework. Furthermore, given the GP model's ability to give time-series prediction, it is worthwhile in the future to incorporate early-age strengths as constraints or targets (as opposed to only 28-day strength) into the optimization framework.

4.5. Incorporation of uncertainty into optimization

Due to the ability of the GP model to estimate the prediction uncertainty, here we explored the possibility to incorporate the prediction uncertainty into the optimization. As outlined in Section 3.3.1, one way to do it is to implement "the predicted strength of a given mix is larger than the design strength with a certain (e.g., 95%) probability" as opposed to "the mean predicted strength is higher than the design strength" used in previous sections. Fig. 14a shows the probability density curves of the predicted strength for all the mixes generated from fifty independent optimization runs (minimizing climate impact only) with the imposed probability constraint, compared with the case of the original constraint. The implementation of this probability constraint increases the mean strength of the optimized mixes by ∼1,300 psi (∼9 MPa), which essentially generates a safety factor. Depending on how conservative the design needs to be, one could also tune this safety factor by changing the probability (e.g., 90%, 95%, or 99%).

Fig. 14b and 14c show how this probability constraint impacts the distribution of climate impact and cost of the optimized mix design (i.e., mix formulation which gives the global minimal of climate impact among the fifty local minima), respectively. It is clear that the probability constraint leads to slightly higher average climate impact (∼1% increase, Fig. 14b) and cost (∼7% increase, Fig. 14c) for the optimized mix formulations. Nevertheless, the average climate impact (∼132 kg CO_2-eq/CY = ∼ 174 kg CO_2-eq/m^3) and cost (∼57 \$/CY = ∼75 \$/m^3) are still ∼60% and ∼20% lower than those of the industry-adopted mixes, which have an average climate impact and cost of ∼305 kg CO_2-eq/CY (∼ 401 kg CO_2-eq/m^3) and ∼68 \$/CY (∼89 \$/m^3), respectively, for concrete mixes with a strength of ∼10,000 psi.

Furthermore, by imposing the 95% probability constraint, the resulting optimal concrete mix exhibits higher early age strengths than the optimal mix design obtained using the original constraint, as illustrated in Fig. 15. This elevation of early age strength, to a certain extent, alleviates the problem of slow strength development for adopting high content of SCMs in concrete design. Overall, this preliminary analysis on probability constraint here has demonstrated the potential of incorporating prediction uncertainty (readily estimated from the GP model) into the computational framework for more realistic concrete mix design.

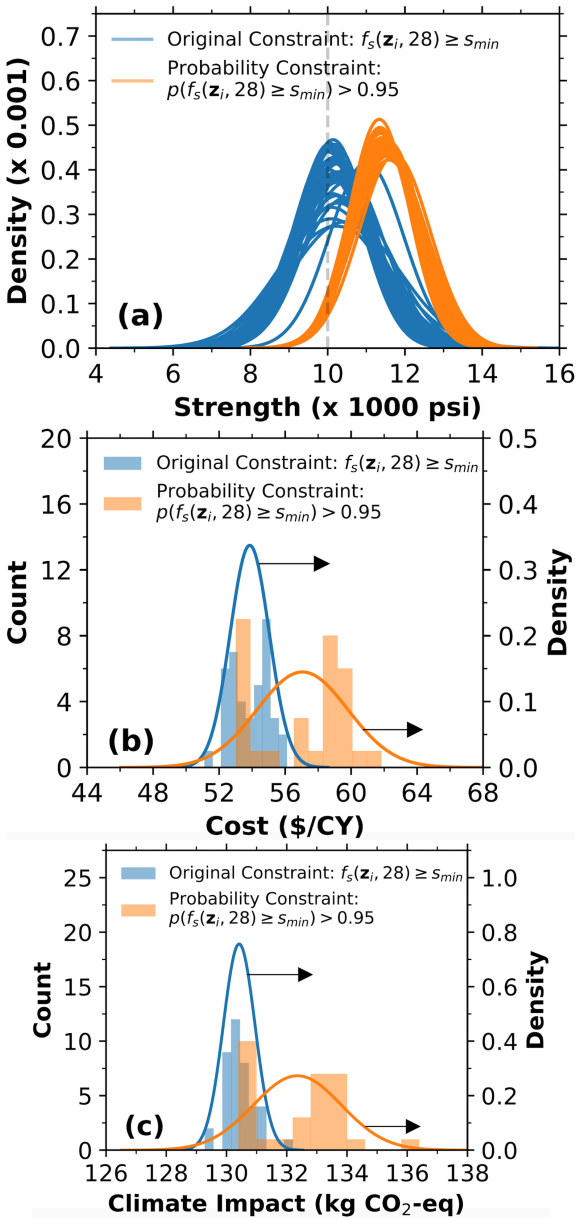

Figure 14: Impact of implementing the probability constraint (i.e, "the predicted strength of a given mix has a 95% probability higher than the target design strength of 10,000 psi") on (a) the strength, (b) climate impact (in kg CO_2-eq/CY), and (c) cost (in $/CY) distribution of the optimized concrete mixes (minimizing climate impact). 10,000 psi = 69.0 MPa; 1 CY = ~0.76 m^3.

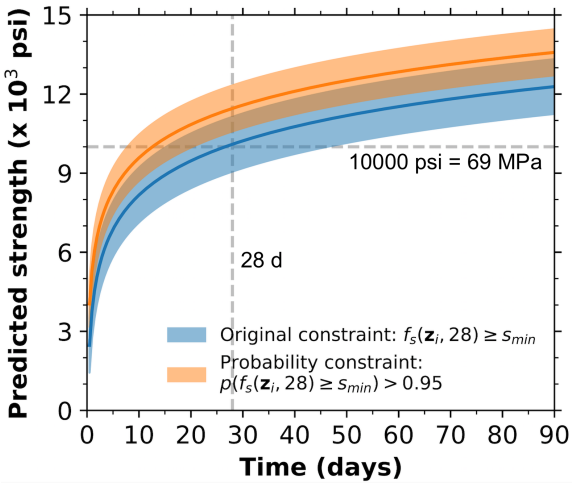

Figure 15: Impact of the imposed probability constraint on the predicted strength trajectory of the optimal mix design (obtained from single-objective optimization of climate impact) for a target 28-day strength of 10,000 psi (69.0 MPa). The 28-day is indicated by the vertical dashed line. The lines in the middle are the average predictions, with the shaded area representing one standard deviation.

5. Broader Impact and Limitations

This study presents an analysis of a large and complex concrete mix design and strength data set (the largest of its kind, as far as we are aware) from the industry. We have shown that it is possible to generate reasonable concrete mix designs with significant reductions in climate impact and cost (compared with industrial mix designs) by combining domain knowledge-informed GP models with an inverse optimization scheme. This integrated computation framework can be readily extended for the design and optimization of increasingly more complex concrete materials, which is likely to be the case in the future concrete industry as the research community is actively exploring a wide range of new SCMs and concrete additives. It also allows optimal solutions to be readily generated for any given cost and climate impact factors (as given in Tables 2 and 3), which are known to evolve with time, source and region. Furthermore, this integrated computation framework might also be extended to study and optimize (i) other important concrete properties which evolve as a function of time (e.g., pore structure, transport properties, and durability) and (ii) other complex materials systems with evolving properties (e.g., batteries).

Nevertheless, a number of limitations of this study warrant some discussion. First, as explained in Section 2, this study focuses on 12 main constituent categories without detailed information on, for example, the chemistry, mineralogy, and particle sizes of different types of cements, BFSs, and FAs used (not available in our data set). This is actually the case for all existing concrete strength data sets and ML-based inverse optimization studies, where the chemical and mineralogical information is not available, as far as we are aware. However, the chemistry, mineralogy, and particle sizes of SCMs [63, 64] and cements [65, 66] (and to some extent, aggregates [67]) can have significant impacts on the mechanical strength of concrete, as well as other properties. Provision of this detailed information would empower these ML models to capture more chemistry and physics, leading to improved property predictions (with lower uncertainty) and hence more realistic mix designs from the inverse optimization process.

Second, the current study uses 28-day compressive strength as the design target (performance requirement), similar to many existing optimization studies. However, there are other equally important performance requirements that concrete design needs to consider. For example, the concrete mixture needs to maintain a certain level of workability (e.g., slump), exhibit proper early-age strength development, and contain a certain amount of entrained air depending on the requirement for freeze and frost resistance for a given application. In the current study, we have done a final check on the early-age strength trajectories of the optimized concrete mix (Section 4.5) and considered scenarios with an imposed constraint on AEA. We have also constrained the aggregate ratio to 0.65-0.75 to avoid generation of mixes with excessively large amount of aggregate, which is known to cause workability issues [51]. Further studies on this data set should explore the incorporation of strength trajectories (as opposed to a single age strength), as well as air content, and slump as the design targets, which would enable the generation of more realistic mix designs.

6. Conclusions

In this work, we developed a data-driven computational framework that can accelerate and optimize concrete mix design with respect to climate impact and/or cost. We first use a large industry concrete data set (containing 9,296 mixes and 38,332 strength measurements collected at different sites across the USA during 2017-2020 by a concrete producer) to develop a novel

amortized Gaussian process (GP) model for predicting concrete strength as a function of mix proportions. In spite of the inherent uncertainty and complexity of the industry data, we show that the domain knowledge-informed GP models give reasonable predictions of strength and strength trajectories with R^2 values of ∼0.88, RMSE of ∼909 psi, and MAPE of ∼10.8%. These error statistics are seen to be comparable to those achieved using random forest and artificial neural network models. Although the prediction accuracy is lower than many published ML models based on smaller and simpler lab data sets, it is higher than that achieved in other ML studies also based on industry concrete strength data.

We then developed an optimization framework based on the GP model that enables rapid generation of concrete mix designs for a given target 28-day strength ranging from 6000 to 13000 psi (∼41.1 to ∼89.7 MPa). Both single-objective (minimize cost or climate impact) and bi-objective (minimize both cost and climate impact) optimization have been carried out subject to bounds and constraints estimated from the raw data. The optimization results demonstrate that this integrated computational framework can be used to generate reasonable mix designs that satisfy set performance requirements (including the target 28-day strength and early-age strength development) while substantially reducing the cost (up to ∼30%) and climate impact (up to ∼60%) compared with industry mixes with similar strength. These reductions are mainly attributed to the generally higher replacement ratio of cement with supplementary cementitious materials (SCMs, up to the set limit of 60%) in the predicted optimal designs than in the industry data, which has an average SCM replacement ratio of ∼16%. This suggests the existence of huge environmental and economic benefits for the data-driven concrete mix optimization (presented here) compared to the prescriptive and trial-and-error approaches commonly used by the industry. Our bi-objective optimization reveals a trade-off between cost and climate impact, with a cost increase of 0.5-1$ for every kg CO_2-eq saved for most of the target strengths. We further showed that the GP model can enable the incorporation of prediction uncertainty into the computational framework, leading to more realistic mix designs. Nevertheless, more research is needed to validate the generated optimal mix designs, further improve the optimization process and overcome its associated limitations.

Finally, in light of the potential price increase of SCMs, we have studied three price increase scenarios, which show that the cost of optimized concrete mixes is more sensitive to the price increase of fly ash (FA) than blast furnace

slag (BFS). The bi-objective optimization shows that this price increase can significantly increase the climate impact of the optimized concrete mixes when cost minimization is heavily weighted. The shortage of high-quality FA and BFS, which are the main SCMs used in the industry currently, highlights the need to develop approaches that enable the utilization of low-quality FAs and BFSs and alternative sources of SCMs (e.g., volcanic ashes, calcined clay, and waste glass powder, just to name a few) by the industry. To achieve this goal, data-driven concrete mix design, as presented in this work, exhibits huge potential given its ability to capture the highly complex mix design-property correlations within increasingly complex concrete systems.

7. Acknowledgments

The work is based on the financial support of the MIT-IBM Watson AI Lab. We thank our industry partner for providing the industry data set.

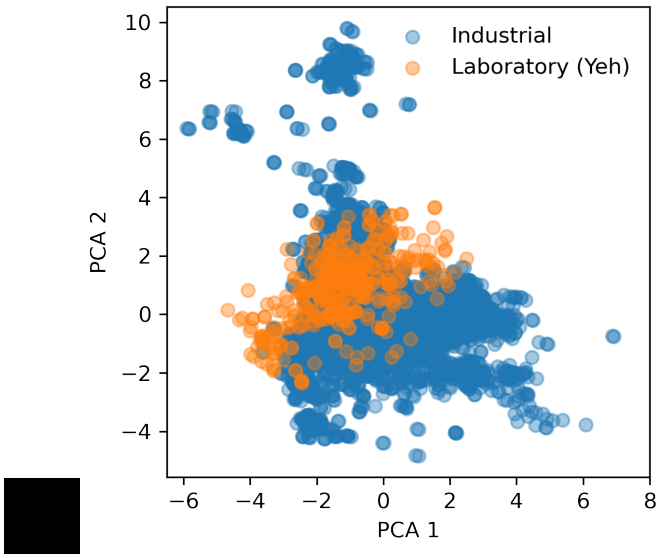

Figure S1: Principle component analysis of our industry data set and the Yeh data set

Appendix A. Supplementary Material

Appendix A.1. Principle component analysis

Principle component analysis (PCA) is statistic method commonly used to lower the dimensionality of high dimensional data set. Here we performed PCA analysis on both our industry data set and the Yeh data set [15]. Fig. S1 shows the results of the first and second principle components, which explain the most variance in the data. The comparison clearly shows that the industry data set contains more variance than the Yeh data set.

Appendix A.2. Correlation between HRWR admixture and w/cm

Fig. S2 compares the HRWR quantity with the corresponding w/cm ratio for all the industry mixes, which shows a general inverse correlation.

Appendix A.3. Gaussian Process Model Constraint Details

As noted in Section 3.1, the prior distribution on compressive strength, y is Gaussian. Therefore, we can use the cumulative distribution function of a

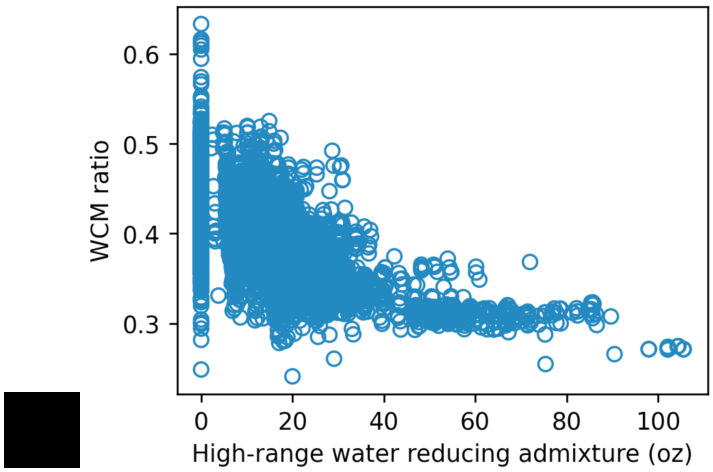

Figure S2: Correlation between quantity of high-range water-reducing (HRWR) admixture and w/cm of all concrete mixes in our industrial data set

Gaussian distribution to calculate the probability that the predicted strength exceeds a threshold value.

$$p(y_i \geq s_{min}|t, \boldsymbol{\theta}_i, \sigma_t, \phi) = 1 - \Phi\Big(\frac{s_{min} - \mu}{\sigma}\Big) \tag{A.1}$$

$$\Phi(x) = \frac{1}{\sqrt{2\pi}} \int_{-\infty}^{x} \exp^{-t^2/2}\, dt \tag{A.2}$$

where μ and σ are the mean and standard deviation of the conditional distribution, respectively.

Appendix A.4. AEA relative to cement

Fig. S3 gives the quantity of total air-entraining admixture (in oz) per 100 lb of cement powder for all the industry mixes, which shows that the most probable ratio is ∼0.39 (oz/100 lb).

Appendix A.5. More details on the single-objective optimization

We used the differential evolution (DE) algorithm, a heuristic optimization algorithm developed by Storn and Price [52], to search for the optimal mix designs in the design space (bounds and constraints in Section 3.3.1) with respect to the objective. Heuristic methods are typically stochastic direct search methods which involve the generation of variations of a candidate

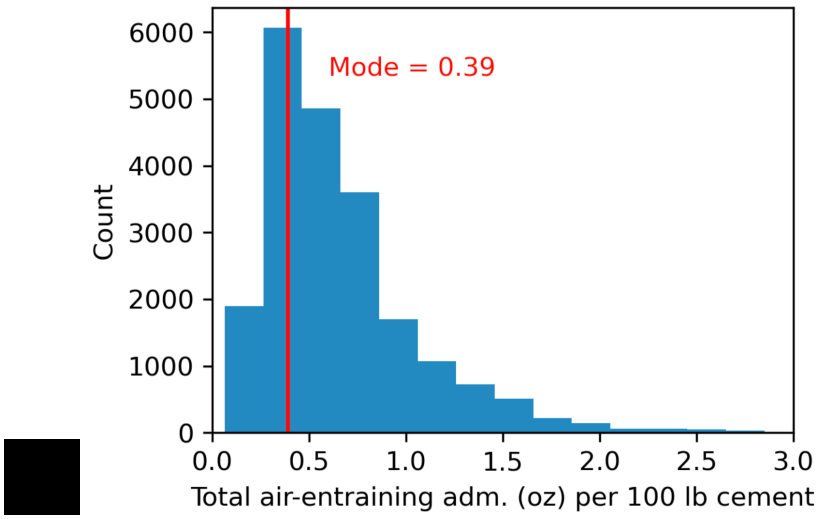

Figure S3: Histogram of the ratio of air-entraining admixture quantity (in oz) per 100 lb of cement for all the air-entrained concrete in the data set.

solution vector. These methods are able to search large spaces with reasonable computation costs. DE is a highly versatile evolutionary algorithm for solving multidimensional and continuous minimization problems. Unlike genetic algorithms, DE is specifically designed for real-valued functions. The full optimizations are summarized in Eqs. A.3 and A.4.

Minimize Climate Impact.

$$
\begin{aligned}
\min \quad & f_g(\mathbf{z}) \\
\text{subject to} \quad & s_{min} \leq f_s(\mathbf{z}, 28) \\
& 0.99 \leq V \leq 1.01 \\
& LB_j \leq z_j \leq UB_j \quad \forall j \\
& 0 \leq R_{SCM} \leq 0.6 \\
& 0 \leq R_{FA} \leq 0.4 \\
& 0 \leq R_{SL} \leq 0.6 \\
& 0 \leq R_{SF} \leq 0.1 \\
& 0.2 \leq R_{WCM} \leq 0.6 \\
& 0.65 \leq V_{agg} \leq 0.75
\end{aligned}
\tag{A.3}
$$

Minimize Cost.

$$
\begin{aligned}
\min \quad & f_c(\mathbf{z}) \\
\text{subject to} \quad & s_{min} \leq f_s(\mathbf{z}, 28) \\
& 0.99 \leq V \leq 1.01 \\
& LB_j \leq z_j \leq UB_j \quad \forall j \\
& 0 \leq R_{SCM} \leq 0.6 \\
& 0 \leq R_{FA} \leq 0.4 \\
& 0 \leq R_{SL} \leq 0.6 \\
& 0 \leq R_{SF} \leq 0.1 \\
& 0.2 \leq R_{WCM} \leq 0.6 \\
& 0.65 \leq V_{agg} \leq 0.75
\end{aligned}
\tag{A.4}
$$

In their study, Storn and Price [52] evaluate the performance of the DE algorithms on ten different optimization test problems, in comparison with two simulated annealing methods, namely Annealed Nelder and Mead (ANM) and Adaptive Simulated Annealing (ASA). Their results, based on 20 minimization runs, revealed that DE successfully finds the global optimum for all ten test problems, while ANM and ASA experienced convergence issues on five and three of the test problems, respectively. Moreover, DE exhibited a tendency to converge in fewer function evaluations compared to ANM and ASA, rendering it advantageous for our work because a large number of highly non-linear constraints makes function evaluation costly.

In this study, we have performed multiple runs (50 runs) of DE at each target strength and preference weighting factor (in the case of bi-objective) to account for the possible impact of the initial guess and increase the diversity of the solutions. We selected the "best" mutation strategy (as opposed to "random") due to the nature of our highly constrained search space (with nine non-linear and one linear constraint) and a large number of decision variables (12). We selected the control parameters, including NP (population size), F (mutation constant controlling diversity amplification within the range of [0,2]), and CR (crossover constant determining the threshold for keeping mutations within the range of [0,1]), following the rules of thumb proposed by Storn and Price. According to their guidelines, NP should be set between 5 and 10 times the number of dimensions of the objective function; thus, we set NP to 15. Selecting a high mutation constant increases the search radius but will slow down convergence. Thus, we have set F to

randomly change between 0.5 and 1 throughout the minimization process in order to speed up convergence. Lastly, large crossover values keep more mutants, which may lead to population instability, while smaller values cause slow convergence. Through trial and error, we have found CR of 0.7 to be a reasonable middle ground.

Appendix A.6. Random forest and multi-layer perceptron models

We trained the random forest (RF) and artificial neural network (ANN) models using the same training set used to train the GP model. The RF model used to generate strength prediction results in Fig. 6b of the main article uses bootstrapping and contains 100 decision trees and a maximum of 3 features at each split, which are determined via hyperparameter tuning.

The multi-layer perceptron (MPL) model used to generate strength prediction results in Fig. 6c of the main article adopt a hidden layer size of (64, 64, 64), a mini-batch size of 200, and the ReLU activation function. We optimized the model weights using the Adam solver [68]. The model converges after 236 iterations based on the specified convergence tolerance (i.e., loss improvement lower than 10^{-4} for 10 consecutive iterations) with a constant learning rate of 0.001.

Appendix A.7. Distribution of optimized constituent quantities in Fig. 9

Appendix A.8. Cost distribution of concrete constituents

Fig. S5 shows the average proportion of cost for the twelve concrete constituent in all the industry mixes. The cost is estimated using the unit price data in Table 3.

Appendix A.9. SCM ratios as a function of design strength

Fig. S6 shows how the ratios of cement replacement with different SCMs (FA, BFS, and FA) evolve as a function of 28-day target strength. These ratios are calculated from the single-objective optimization results in Fig. 9.

Appendix A.10. More details about Fig. 11 of the main article

Fig. S7 shows the bi-objective optimization results for the 9,000 psi target strength, as a weighting factor of 0 (minimizing cost only) and 0.1.

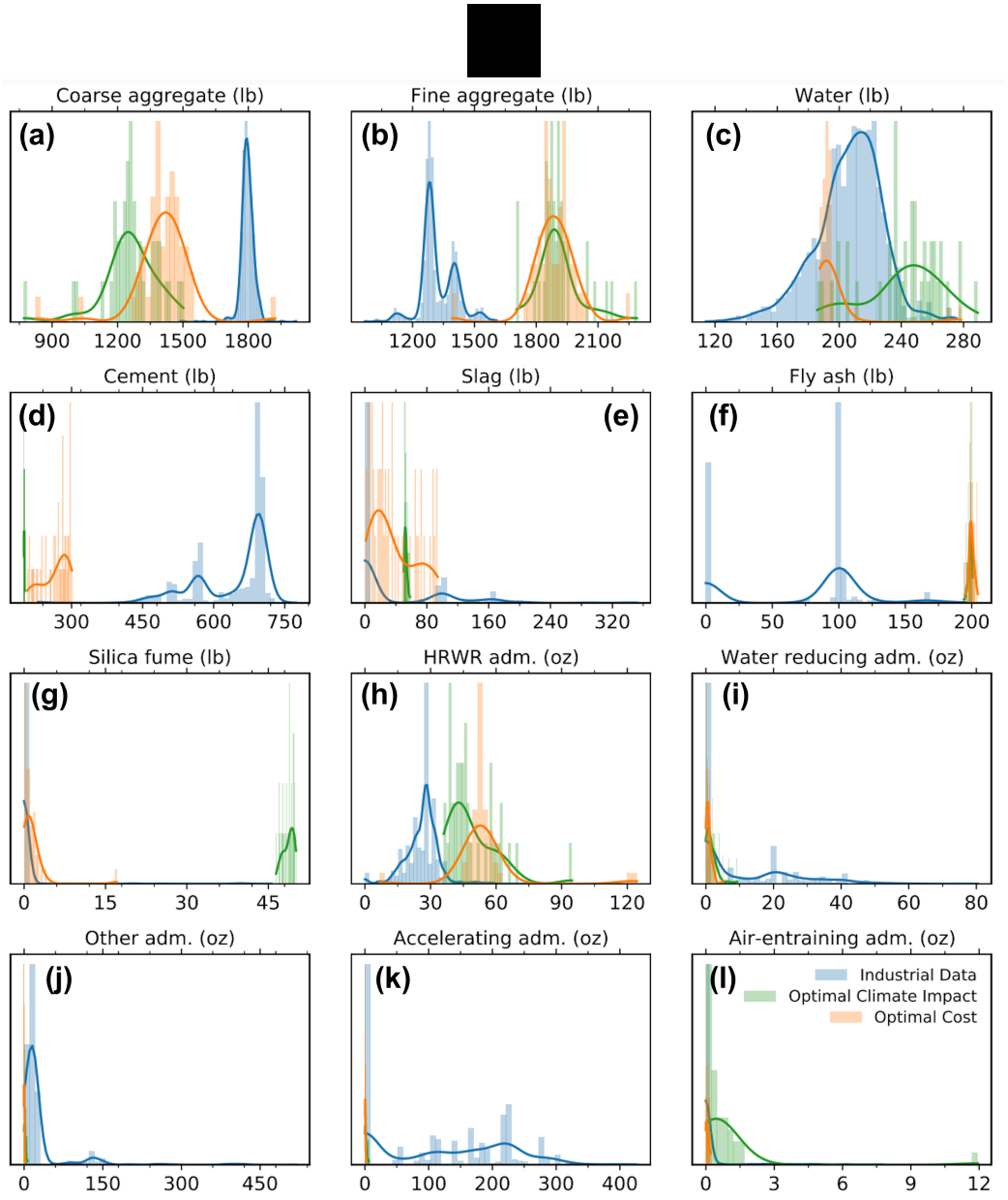

Figure S4: Distribution of the quantities of each constituent (as labelled in each figure) in the optimized concrete mixes (based on 50 runs) for schemes i (minimizing cost) and ii (minimizing climate impact) and a target strength of 10,000 psi (69 MPa) in Fig. 9. The distribution of the constituent quantities of the industry mix designs in our database with strength in the range of 10,000-11,000 psi (69-75.9 MPa) are given in the figures (light blue) for comparison. 1 lb = 0.45 kg; 1 oz = 0.028 kg.

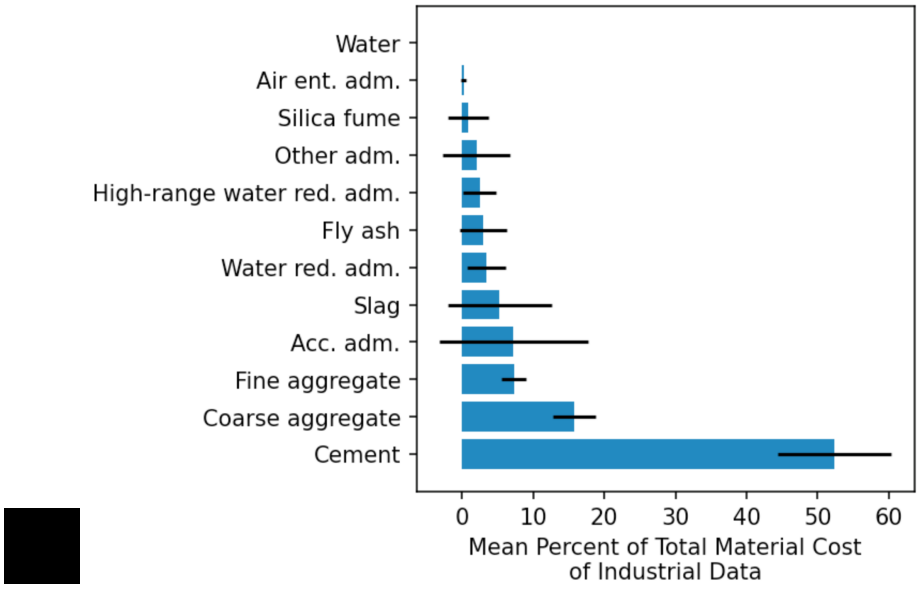

Figure S5: Average percentage cost of each concrete constituent, based all the industry mix formulations. The error bars are one standard deviation.

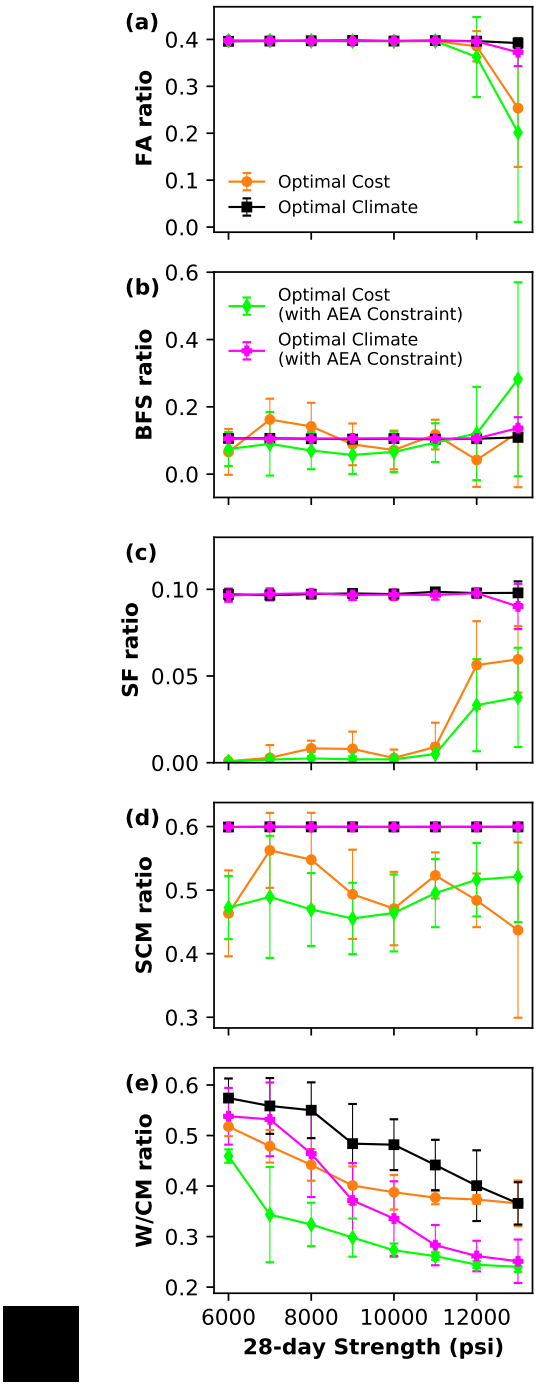

Figure S6: Evolution of (a) FA replacement ratio, (b) BFS replacement ratio, (c) SF replacement ratio, (d) total SCM ratio, and (e) W/CM ratio of the optimized concrete mixes calculated based on the optimization results in Fig. 9. as a function of the target design strength in psi (1000 psi = 6.9 MPa).

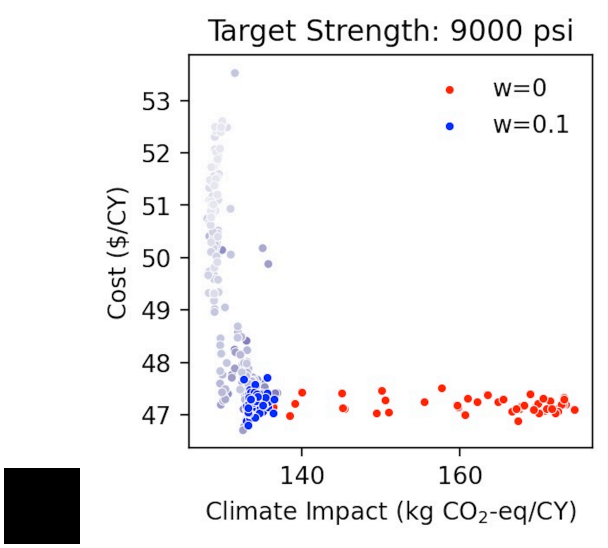

Figure S7: Comparison of the cost-climate impact of the fifty independent production runs for a weight factor of 0 (red) and 0.1 (blue).

References

[1] P. J. M. Monteiro, S. A. Miller, A. Horvath, Towards sustainable concrete, Nat. Mater. 16 (2017) 698–699.

[2] K. Daehn, R. Basuhi, J. Gregory, M. Berlinger, V. Somjit, E. A. Olivetti, Innovations to decarbonize materials industries, Nat. Rev. Mater. 7 (2022) 275–294.

[3] L. Barcelo, J. Kline, G. Walenta, E. Gartner, Cement and carbon emissions, Mater. Struct. 47 (2014) 1055–1065.

[4] L. D. Ellis, A. F. Badel, M. L. Chiang, R. J.-Y. Park, Y.-M. Chiang, Toward electrochemical synthesis of cement—an electrolyzer-based process for decarbonating $CaCO_3$ while producing useful gas streams, Proc. Natl. Acad. Sci. U.S.A. 117 (2020) 12584–12591.

[5] J. Lehne, F. Preston, Making concrete change: Innovation in low-carbon cement and concrete, 2018.

[6] B. A. Young, A. Hall, L. Pilon, P. Gupta, G. Sant, Can the compressive strength of concrete be estimated from knowledge of the mixture proportions?: New insights from statistical analysis and machine learning methods, Cem. Concr. Res. 115 (2019) 379–388.

[7] M. DeRousseau, E. Laftchiev, J. Kasprzyk, B. Rajagopalan, W. Srubar III, A comparison of machine learning methods for predicting the compressive strength of field-placed concrete, Constr. Build. Mater. 228 (2019) 116661.

[8] X. Zhang, M. Z. Akber, W. Zheng, Prediction of seven-day compressive strength of field concrete, Constr. Build. Mater. 305 (2021) 124604.

[9] M. C. G. Juenger, R. Snellings, S. A. Bernal, Supplementary cementitious materials: New sources, characterization, and performance insights, Cem. Concr. Res. 122 (2019) 257–273.

[10] M. C. G. Juenger, R. Siddique, Recent advances in understanding the role of supplementary cementitious materials in concrete, Cem. Concr. Res. 78 (2015) 71–80.

[11] M. A. DeRousseau, J. R. Kasprzyk, W. V. Srubar III, Computational design optimization of concrete mixtures: A review, Cem. Concr. Res. 109 (2018) 42–53.

[12] W. Ben Chaabene, M. Flah, M. L. Nehdi, Machine learning prediction of mechanical properties of concrete: Critical review, Constr. Build. Mater. 260 (2020) 119889.

[13] I. Nunez, A. Marani, M. Flah, M. L. Nehdi, Estimating compressive strength of modern concrete mixtures using computational intelligence: A systematic review, Constr. Build. Mater. 310 (2021) 125279.

[14] Z. Li, J. Yoon, R. Zhang, F. Rajabipour, W. V. Srubar III, I. Dabo, A. Radlińska, Machine learning in concrete science: applications, challenges, and best practices, npj Comp. Mater. 8 (2022) 1–17.

[15] I.-C. Yeh, Modeling of strength of high-performance concrete using artificial neural networks, Cem. Concr. Res. 28 (1998) 1797–1808.

[16] A. Behnood, E. M. Golafshani, Predicting the compressive strength of silica fume concrete using hybrid artificial neural network with multi-objective grey wolves, J. Clean. Prod. 202 (2018) 54–64.

[17] D.-K. Bui, T. Nguyen, J.-S. Chou, H. Nguyen-Xuan, T. D. Ngo, A modified firefly algorithm-artificial neural network expert system for predicting compressive and tensile strength of high-performance concrete, Constr. Build. Mater. 180 (2018) 320–333.

[18] J.-S. Chou, C.-K. Chiu, M. Farfoura, I. Al-Taharwa, Optimizing the prediction accuracy of concrete compressive strength based on a comparison of data-mining techniques, J. Comp. Civil Eng. 25 (2011) 242–253.

[19] D.-C. Feng, Z.-T. Liu, X.-D. Wang, Y. Chen, J.-Q. Chang, D.-F. Wei, Z.-M. Jiang, Machine learning-based compressive strength prediction for concrete: An adaptive boosting approach, Constr. Build. Mater. 230 (2020) 117000.

[20] P. G. Asteris, A. D. Skentou, A. Bardhan, P. Samui, K. Pilakoutas, Predicting concrete compressive strength using hybrid ensembling of surrogate machine learning models, Cem. Concr. Res. 145 (2021) 106449.

[21] K. Severson, O. Pfeiffer, J. Chen, K. Gong, J. Gregory, R. Goodwin, E. Olivetti, Amortized inference of gaussian process hyperparameters for improved concrete strength trajectory prediction, in: NeurIPS 2021 Workshop on Tackling Climate Change with Machine Learning, 2021.

[22] M. Simon, Concrete mixture optimization using statistical methods: final report, 2003.

[23] I.-C. Yeh, Computer-aided design for optimum concrete mixtures, Cem. Concr. Comp. 29 (2007) 193–202.

[24] T. Kim, S. Tae, S. Roh, Assessment of the CO_2 emission and cost reduction performance of a low-carbon-emission concrete mix design using an optimal mix design system, Renew. Sust. Energ. Rev. 25 (2013) 729–741.

[25] M. H. Rafiei, W. H. Khushefati, R. Demirboga, H. Adeli, Novel approach for concrete mixture design using neural dynamics model and virtual lab concept., ACI Mater. J. 114 (2017).

[26] T. Ji, Y. Yang, M.-y. Fu, B.-c. Chen, H.-C. Wu, Optimum design of reactive powder concrete mixture proportion based on artificial neural and harmony search algorithm., ACI Mater. J. 114 (2017).

[27] Y. Huang, J. Zhang, F. Tze Ann, G. Ma, Intelligent mixture design of steel fibre reinforced concrete using a support vector regression and firefly algorithm based multi-objective optimization model, Constr. Build. Mater. 260 (2020) 120457.

[28] J. Zhang, Y. Huang, Y. Wang, G. Ma, Multi-objective optimization of concrete mixture proportions using machine learning and metaheuristic algorithms, Constr. Build. Mater. 253 (2020) 119208.

[29] I. Nunez, A. Marani, M. L. Nehdi, Mixture optimization of recycled aggregate concrete using hybrid machine learning model, Mater. 13 (2020) 4331.

[30] S. A. T. Motlagh, M. Naghizadehrokni, An extended multi-model regression approach for compressive strength prediction and optimization of a concrete mixture, Constr. Build. Mater. 327 (2022) 126828.

[31] X. Ge, R. T. Goodwin, H. Yu, P. Romero, O. Abdelrahman, A. Sudhalkar, J. Kusuma, R. Cialdella, N. Garg, L. R. Varshney, Accelerated design and deployment of low-carbon concrete for data centers, arXiv preprint arXiv:2204.05397 (2022).

[32] J. Zhang, Y. Huang, F. Aslani, G. Ma, B. Nener, A hybrid intelligent system for designing optimal proportions of recycled aggregate concrete, J. Clean Prod. 273 (2020) 122922.

[33] F. Dabbaghi, A. Tanhadoust, M. Nehdi, S. Nasrollahpour, M. Dehestani, H. Yousefpour, Life cycle assessment multi-objective optimization and deep belief network model for sustainable lightweight aggregate concrete, J. Clean. Prod. 318 (2021) 128554.

[34] S. Popovics, J. Ujhelyi, Contribution to the concrete strength versus water-cement ratio relationship, J. Mater. Civil Eng. 20 (2008) 459–463.

[35] R. Duval, E. H. Kadri, Influence of silica fume on the workability and the compressive strength of high-performance concretes, Cem. Concr. Res. 28 (1998) 533–547.

[36] S. Bhanja, B. Sengupta, Influence of silica fume on the tensile strength of concrete, Cem. Concr. Res. 35 (2005) 743–747.

[37] H. A. Shah, Q. Yuan, S. Zuo, Air entrainment in fresh concrete and its effects on hardened concrete-a review, Constr. Build. Mater. 274 (2021) 121835.

[38] S. Roberts, M. Osborne, M. Ebden, S. Reece, N. Gibson, S. Aigrain, Gaussian processes for time-series modelling, Philos. Trans. Royal Soc. A 371 (2013) 20110550.

[39] G. Wernet, C. Bauer, B. Steubing, J. Reinhard, E. Moreno-Ruiz, B. Weidema, The ecoinvent database version 3 (part I): overview and methodology, Int. J. Life Cycle Assess. 21 (2016) 1218–1230.

[40] A cradle-to-gate life cycle assessment of ready-mixed concrete manufactured by NRMCA members – version 3, 2020.

[41] European Federation of Concrete Admixtures Associations Ltd. (EFCA), Environmental product declaration - concrete admixtures – set accelerators, 2015.

[42] European Federation of Concrete Admixtures Associations Ltd. (EFCA), Environmental product declaration - concrete admixtures – air entrainers, 2015.

[43] European Federation of Concrete Admixtures Associations Ltd. (EFCA), Environmental product declaration - concrete admixtures – plasticisers and superplasticisers, 2015.

[44] Portland Cement Association, Environmental product declaration portland cement, 2021.

[45] T. García-Segura, V. Yepes, J. Alcalá, Life cycle greenhouse gas emissions of blended cement concrete including carbonation and durability, Int. J. Life Cycle Assess. 19 (2014) 3–12.

[46] L. Bushi, J. Meil, G. Finlayson, An industry average cradle-to-gate life cycle assessment of slag cement for the USA and canadian markets, 2021.

[47] D. Wałach, P. Dybeł, J. Sagan, M. Gicala, Environmental performance of ordinary and new generation concrete structures—a comparative analysis, Environ. Sci. Pollut. Res. 26 (2019) 3980–3990.

[48] K. M. Rahla, R. Mateus, L. Bragança, Comparative sustainability assessment of binary blended concretes using supplementary cementitious materials (SCMs) and ordinary portland cement (OPC), J. Clean. Prod. 220 (2019) 445–459.

[49] J. Zhang, Y. Huang, G. Ma, B. Nener, Mixture optimization for environmental, economical and mechanical objectives in silica fume concrete: A novel frame-work based on machine learning and a new meta-heuristic algorithm, Resour. Conserv. Recycl. 167 (2021) 105395.

[50] L. H. Jiang, V. M. Malhotra, Reduction in water demand of non-air-entrained concrete incorporating large volumes of fly ash, Cem. Concr. Res. 30 (2000) 1785–1789.

[51] P. J. M. Monteiro, P. R. L. Helene, S. H. Kang, Designing concrete mixtures for strength, elastic modulus and fracture energy, Mater. Struct. 26 (1993) 443–452.

[52] R. Storn, K. Price, Differential evolution – a simple and efficient heuristic for global optimization over continuous spaces, J. Glob. Optim. 11 (1997) 341–359.

[53] P. Virtanen, R. Gommers, T. E. Oliphant, M. Haberland, T. Reddy, D. Cournapeau, E. Burovski, P. Peterson, W. Weckesser, J. Bright, S. J. van der Walt, M. Brett, J. Wilson, K. J. Millman, N. Mayorov, A. R. J. Nelson, E. Jones, R. Kern, E. Larson, C. J. Carey, İ. Polat, Y. Feng, E. W. Moore, J. VanderPlas, D. Laxalde, J. Perktold, R. Cimrman, I. Henriksen, E. A. Quintero, C. R. Harris, A. M. Archibald, A. H. Ribeiro, F. Pedregosa, P. van Mulbregt, SciPy 1.0 Contributors, Scipy 1.0: Fundamental algorithms for scientific computing in python, Nat. Methods 17 (2020) 261–272.

[54] R. Marler, J. Arora, Survey of multi-objective optimization methods for engineering, Struct. Multidiscipl. Optim. 26 (2004) 369–395.

[55] G. Habert, D. Arribe, T. Dehove, L. Espinasse, R. Le Roy, Reducing environmental impact by increasing the strength of concrete: quantification of the improvement to concrete bridges, J. Clean Prod. 35 (2012) 250–262.

[56] G. Xu, Q. Tian, J. Miao, J. Liu, Early-age hydration and mechanical properties of high volume slag and fly ash concrete at different curing temperatures, Constr. Build. Mater. 149 (2017) 367–377.

[57] R. Demirboğa, İ. Türkmen, M. B. Karakoc, Relationship between ultrasonic velocity and compressive strength for high-volume mineral-admixtured concrete, Cem. Concr. Res. 34 (2004) 2329–2336.

[58] A. Gholampour, T. Ozbakkaloglu, Performance of sustainable concretes containing very high volume Class-F fly ash and ground granulated blast furnace slag, J. Clean. Prod. 162 (2017) 1407–1417.

[59] T. Lee, J. Lee, Y. Kim, Effects of admixtures and accelerators on the development of concrete strength for horizontal form removal upon curing at 10 °C, Constr. Build. Mater. 237 (2020) 117652.

[60] H. Yoon, Y. J. Kim, H. S. Kim, J. W. Kang, H.-M. Koh, Evaluation of early-age concrete compressive strength with ultrasonic sensors, Sensors 17 (2017) 1817.

[61] B. Standards, Structural Use of Concrete: Part 1: Code of Practice for Design and Construction, British Standards Institution, 2007.

[62] B. S. EN, 206-1 concrete-part 1: Specification, performance, production and conformity, British Standards Institution (2000).

[63] J. Skibsted, R. Snellings, Reactivity of supplementary cementitious materials (SCMs) in cement blends, Cem. Concr. Res. 124 (2019) 105799.

[64] K. Gong, C. E. White, Predicting CaO-(MgO)-Al_2O_3-SiO_2 glass reactivity in alkaline environments from force field molecular dynamics simulations, Cem. Concr. Res. 150 (2021) 106588.

[65] Z. Osmanovic, N. Haračić, J. Zelić, Properties of blastfurnace cements (CEM III/A, B, C) based on portland cement clinker, blastfurnace slag and cement kiln dusts, Cem. Concr. Compos. 91 (2018) 189–197.

[66] B. Kipkemboi, T. Zhao, S. Miyazawa, E. Sakai, N. Nito, H. Hirao, Effect of C3S content of clinker on properties of fly ash cement concrete, Constr. Build. Mater. 240 (2020) 117840.

[67] B. M. Aïssoun, S.-D. Hwang, K. H. Khayat, Influence of aggregate characteristics on workability of superworkable concrete, Mater. Struct. 49 (2016) 597–609.

[68] D. P. Kingma, J. Ba, Adam: A method for stochastic optimization, arXiv preprint arXiv:1412.6980 (2014).